Experimental and numerical study of open bath immersion cooling of microprocessors.

By

Amirreza Niazmand

Presented to the Faculty of the Graduate School of

The University of Texas at Arlington in Partial Fulfillment

of the Requirements

for the Degree of

DOCTOR OF PHILOSOPHY

THE UNIVERSITY OF TEXAS AT ARLINGTON

August 2020

Supervising Committee:

Dr. Dereje Agonafer, (Supervising Professor)

Dr. Abdolhossein Haji-Sheikh

Dr. Zeynep Çelik-Butler

Dr. Miguel Amaya

Dr. Amir Ameri

Copyright © by Amirreza Niazmand 2020

All Rights Reserved

Acknowledgements

I would like to take this opportunity to thank my supervising professor, Prof. Dereje Agonafer, for his constant encouragement, support and guidance during the course of my research and studies at this University. The invaluable advice and support provided by him was the major driving force, which enabled me to complete my dissertation.

I would like to thank Dr. Haji-Sheikh, Dr. Buttler, Dr. Ameri and Dr. Amaya for taking time to serve on my dissertation committee.

Also, I would like to thank Dr. Shayesteh and Dr. Ameri for helping me through additive manufacturing of the parts.

I would like to thank Mr. Kermit Beird and Mr. Sam Williams for their help with equipment fabrication.

I would like to thank Dr. Jalal Fathi and all my friends in the EMNSPC team and in the University for helping me throughout my time here at this University.

Finally, I would like to thank my parents for their support, both emotionally and financially, without which I would not have been able to complete my degree.

Dedication

I would like to dedicate my PhD Dissertation

To

My parents

Zohre and Mehdi,

For their love, endless support and encouragement.

To

The best friend and sister God ever made,

Mercedeh,

Whose words of encouragement and push for tenacity ring in my ears.

Abstract

The increase on demand of communication and networking has resulted to increase for more powerful servers and bigger data centers. With increase the power of electronics, thermal management and cooling of the equipment become a gigantic challenge due to lower surface, they have higher power density and traditional methods of cooling become ineffective. Generally, air cooling method is the first option for cooling of the electronics due to cheaper price. To increase the efficiency and capacity of cooling liquid immersion cooling is used due to higher thermal properties like heat capacity and thermal conductivity compare to air. Two methods of immersion cooling can be used. The first one is the closed cycle cooling which uses flow boiling which still needs extra power for cooling to circulate the liquid inside the rack. The problem of using this method is that it is not easy to get out of a server for checking or maintenance. Furthermore, to move one server, we need to shut down all servers and wait till the system is cool down. Due to high pressure inside pipes,

the leakage can happen in the system and the liquid which is very expensive must be substituted in the system. Also, the vapor can be trapped in the tank and removing vapor is not easy and during the operation, it can influence the thermal management of the system. The second method is the open bath method which simply, the servers can be submerged in the tank and the maintenance can be done from the opening of the tank. To increase the performance of cooling in this method, enhanced surface should be used on the surface of the processors.

This study explores the cooling performance of 1cm by 1cm dyes which are placed in the different configurations. To make the dyes, a resistance was used and a copper plate is put on top of the heater. A thermocouple is designed in the center of the copper plate to measure the temperature of the surface. An open-bath test cell is designed with two condensers. The temperature of the bath is controlled with a hot plate at the bottom of the cell. To control the temperature inside the bath, a thermocouple is designed inside the bath. To make sure that the temperature is steady state, the results were taken after being sure that the temperature did not change any more. Pool boiling tests were performed on test boards which is able to make different configurations. The proposed work includes 3 different steps. In the first step, the effect of thermal shadowing will be checked to study the effect of bubble columns earlier dyes on the top dyes. For the 2nd steps, the effect of the front space on the surface temperature of the dyes will be checked by adding a glass wall in front

of heater. In the last stage, the effect of surface enhancement will be studied. The surface enhancement is studied by adding micro particles on top of the copper plates, adding lattice structure on top of the heaters. The results will be presented in the form of characteristics curve of boiling which is the heat flux versus surface temperature. The critical heat flux of each configurations and surface will be found. Also, the heat convection coefficient of each configuration will be presented as a curve. To check the boiling phenomena, the photos of bubbles at the surface will be taken and it will be tried to find the bubble departure diameter of the surface.

Contents

Acknowledgements..

Dedication..

Abstract ....

Figures..

Tables..

Nomenclature ....

Chapter 1: Introduction 1

1.1. Cooling of data centers 5

Chapter 2 : Two-phase immersion cooling 17

2.1. Literature review.. 17

2.2. Numerical analyses.. 23

2.3. Simulation setup and boundary conditions.. 29

2.4. Result and Discussion 32
2.4.1 Validation case 32
2.4.2 Single and double CPUs 36
2.4.3 Single Die 40
2.4.4 Side by side configuration of the die 43
2.4.5 Vertical configuration 46
Chapter 3 Test cell design 48
3.1. Results 57
3.1.1 Horizontal uncontrolled bath 58
3.2. Thermal Shadow experiment 61
3.3. Confined space 63
3.4. 3D printed surface 65
3.5. Conclusion 67
References 68
Biography 75

Figures

Figure 1: Growth of data versus time[1].. 2

Figure 2: power density of the CPUs versus size of the transistors[2] 3

Figure 3: increasing rack power versus time 4

Figure 4: projection of the data centers power consumption based on the results of 2014 [3]. 5

Figure 5: a typical air cooled data center[5].. 6

Figure 6 : Cooling approaches: Efficiency vs Density [6]................................ 7

Figure 7: piping of liquid cold plate[7] 8

Figure 8:indirect liquid, cold plate[7] 8

Figure 9: cooling loops of single-phase immersion cooling[8] 9

Figure 10: open bath of single-phase cooling[8].. 9

Figure 11: Schematic diagram for single phase immersion cooling [10] 10

Figure 12: Efficiency of the different cooling methods[18] 12

Figure 13: two immersion cooling of a GIGABYTE computer[19]................. 12

Figure 14: tank and server blades schematic for open bath immersion cooling 13
Figure 15: Schematic of two-phase open bath immersion cooling 14
Figure 16: characteristic curve of boiling [21](heat flux vs wall superheat temperature) 18
Figure 17: the chamber geometry for validation case and boundary conditions 33
Figure 18: Isosurface of 10% vapor volume fraction colored by the velocity . 35
Figure 19: saturation boiling curve of FC-72 for validation case 35
Figure 20: Domain geometry and Boundary conditions 37
Figure 21: Isosurface of vapor volume fraction over chipsets 37
Figure 22:distribution of volume fraction over the chipsets (bottom:4W/cm^2, top:15W/cm^2). 39
Figure 23: Effects of different inclinations on simulated boiling curves of the bottom chipsets 40
Figure 24: configuration and boundary condition of a single die in vertical condition 41
Figure 25: results of single die 10x10mm with vertical condition 42
Figure 26: side by side configuration simulation using symmetry boundary condition 44
Figure 27: results of side by side configuration 10x10mm die 45
Figure 28: vertical configuration of two dies and boundary conditions 46
Figure 29: results of vertical configuration boiling 47

Figure 30: schematic of open bath test cell 49

Figure 31: designed test cell for open bat immersion cooling test 50

Figure 32: designed copper plate as simulated processor 52

Figure 33: right, the cross section of heater and frame. Left, simulation of the design frame. 54

Figure 34: the isothermal lines through middle of the heater and heater frame 54

Figure 35: surface roughness of an intel Xeon CPU 55

Figure 36: surface roughness of copper plate before polish.......................... 56

Figure 37: surface roughness of copper plate after polish............................ 56

Figure 38: bubble generation on the plane surface for the power density (1 W/cm^2) 59

Figure 39: bubble generation on the plane surface for the power density (4 W/cm^2) 59

Figure 40: bubble generation on the plane surface for the power density (10 W/cm^2) 60

Figure 41: bubble generation on the vertical configuration of the plane surface for the power density 4 W/cm^2 62

Figure 42: boiling characteristic curve for vertical configuration 63

Figure 43: vertical configuration with confined space made with glasses 64

Figure 44: boiling characteristic curve for vertical configuration with confined space 64

Figure 45: 3D printed surface with high roughness to increase the efficiency66

Figure 46: comparison of the 3D printed enhanced surface with plane surface
.... 66

Tables

Table 1: Properties of the liquid used in immersion cooling [20] 15

Table 2: Properties of the liquid used in immersion cooling [20] 16

Table 3: Thermal properties of FC-72 at boiling temperature [13]................. 31

Table 4: thermal conductivity of material used in the heater frame 55

Table 5: comparison of the uncontrolled bath temperature 61

Nomenclature

W	Watt
h	heat transfer coefficient, ($W/m^2 \cdot K$)
A	heat transfer area (m^2)
T_s	temperature of the surface (°C)
T_∞	temperature of the fluid (°C)
q''	surface heat flux (W/m^2) or (W/cm^2)
ΔT	temperature difference (°C)
μ	dynamic viscosity (kg.m/sec)
ρ	density (kg/m^3)
Pr	Prandtl number
T_w	wall temperature (°C)

T_{sat}	saturation temperature of the liquid (°C)
C_p	specific heat (kJ/kg·K)
h_{lv}	latent heat of vaporization (kJ/kg)
g	acceleration due to gravity (m/s^2)
C_{sf}	Rohsenow correlation surface constant factor
σ	surface tension (N/m)
P	pressure (kPa)
δ	momentum boundary layer thickness (m)
δ_t	thermal boundary layer thickness (m)
Re	Reynolds number

Subscripts

l	liquid phase property
v	vapor phase property
e	effective

Chapter 1: Introduction

Today, human society progress into the prime of the information age is accelerated and the networking and communication infrastructure needs to be improved rapidly. The capability of digital technologies has helped human to make an interconnected world which networking has become one of the important parts of world economy and without e-commerce, clouds, media storage, PCs and personal electronic devices, the world is not imaginable and the demand is going higher. Figure 1shows the growth of data from 1960 till now. At the beginning of digital revolution, the maximum amount data was 1 MB and in 20 years, the stored data became tenfold but after this period, just in 10 years, the amount of data became 100MB and till now, due to internet of things the amount of stored data is becoming 50BB. These demands have resulted to increase the number, size and power of data centers. On the other hand, the demand for the faster network and electronic devices have led to

developing of electronic devices with higher computational power due to development of microprocessor with higher power densities.

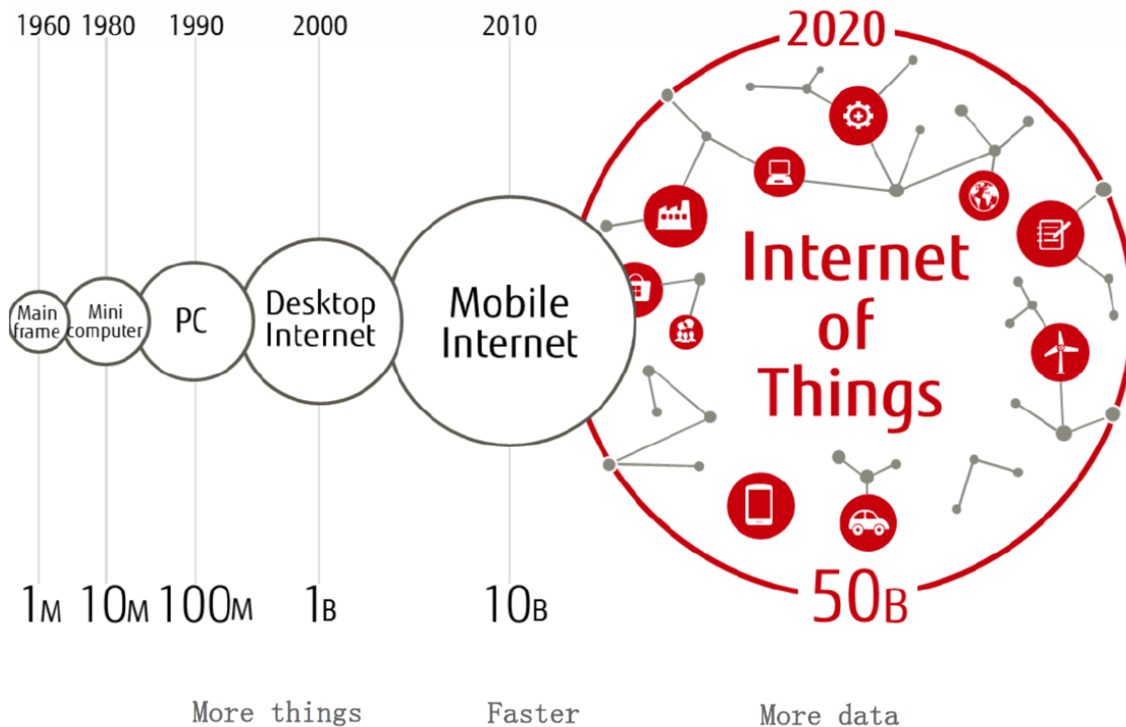

Figure 1: Growth of data versus time[1]

Figure 2 shows the power density of the processors versus the size of the transistors[2]. As this figure shows by using smaller transistor which leads to place more transistor in a processor, the power density of the CPUs increases. The first generation of Intel Pentium had power density of 8 W/cm^2. But the core i7 processor which is almost new processor has power density of about 90 W/cm^2 and it is expected to have to have CPUs with higher power densities even more than 150 W/cm^2.

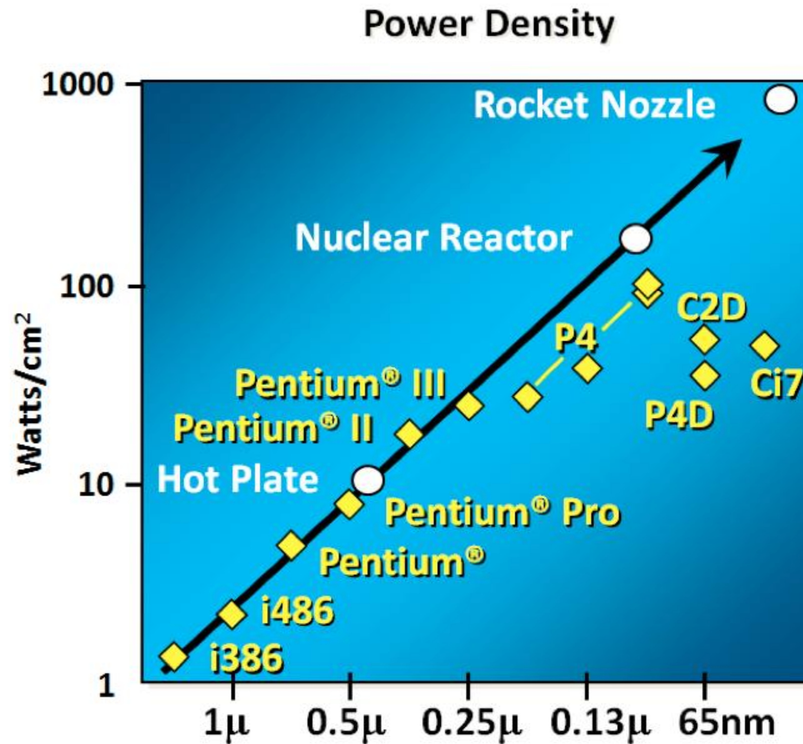

Figure 2: power density of the CPUs versus size of the transistors[2]

The amount of power consumed by a rack in data centers has increases 50 percent from 2010 to 2020. Also, by changing the configuration of the servers in a rack, the power consumption of max configuration is 2.5 times higher than typical configuration. Figure 3 shows the evolution of the rack power in recent years. This improvement of the rack power consumption has leaded to increase in electricity consumption of data centers. In 2014, the total power consumed by the data centers in the US was about 70 billion-kWh. This is roughly 2% of the total electricity power production of the US. By developing new technology, media streaming and electronic trades, the demand for the

new data centers will be increased and its predicted that by 2050, the power consumption of the data centers reach about 180 billion kWh.

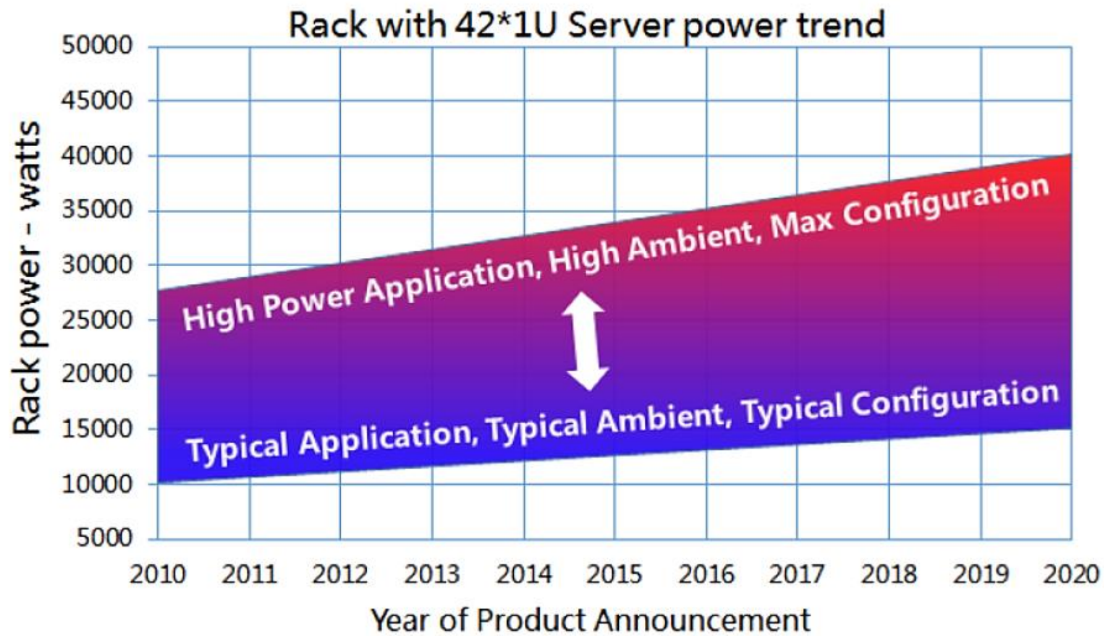

Figure 3: increasing rack power versus time

Figure 4 shows the predicted trend of the power consumption of data centers in the US [3]. In this figure, the flat region after 2008 happened due to recession and after 2011, it became increasing again. Between 2020 to 2030, because of new cooling technologies and manufacturing of servers with higher performances, it is predicted to see reduction in the consumption of electricity and after 2030, the consumption of the power in data centers will be increased dramatically. One of the reasons about this prediction might be due to lack of technology to cool down the servers.

1.1. Cooling of data centers

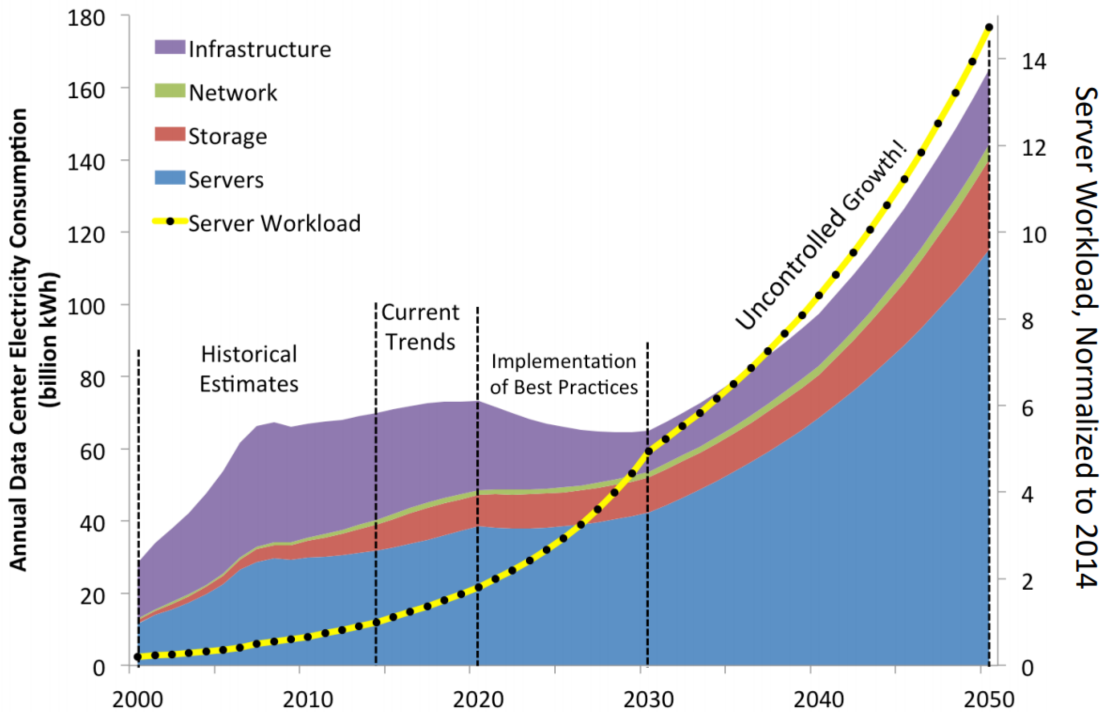

Figure 4: projection of the data centers power consumption based on the results of 2014 [3].

Air cooling is extensively used for cooling of electronics devices. The fan blows air through hot components and it absorbs heat. The hot air is collected in ceiling through ducts. This air is then cooled down by other systems like air handling units or chillers and reinjected back to components through ducts and perforated floor. Figure 5 shows a typical air-cooled data center with hot aisle and cold aisle. The limitation of using air for high-power system is that the air has low thermal properties and it means to remove more heat from the

components, with this it requires higher mass flowrate and higher velocity which increase the energy consumption[4].

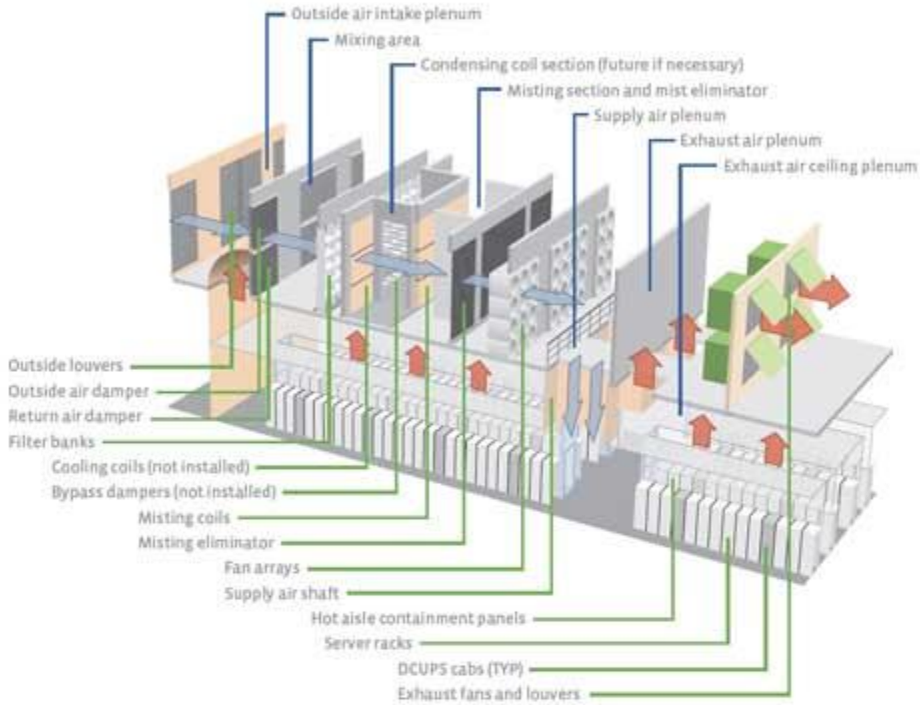

Figure 5: a typical air cooled data center[5]

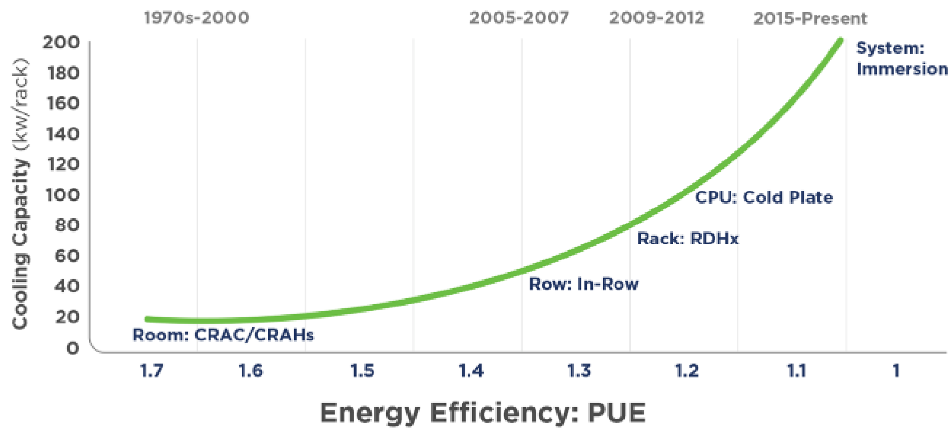

Figure 6 : Cooling approaches: Efficiency vs Density [6]

For higher power density, which could not be cooled with air cooling, next available technology is indirect liquid cooling. Indirect liquid cooling uses cold plate, mounted on the active chip to absorb heat. Liquid coolant is circulated through cold plates, which absorbs and carries heat to heat exchanger and ultimately is dissipated to ambience. Dynamic cold plates could be used to control and regulate the flow rate distribution to hot spot on multi-chip module and further push the capability and make it efficient [2]. Figure 7and Figure 8 show the indirect cooling equipment. Figure 7 show the piping through the servers and Figure 8 shows the cold plate which is attached to the CPU to remove heat from the top surface of it. One of the cons of this method is the highest price of investment and risk of short circuit on the equipment.

Figure 7: piping of liquid cold plate[7]

Figure 8:indirect liquid, cold plate[7]

Capabilities of air cooling could be expanded by adding in row cooler and rear door heat exchanger up to approximately 35 kW per rack. For higher power density, from 35-60 kW per rack approximately, indirect liquid coiling is dominant cooling method for data centers. Beyond this power density per rack, direct liquid cooling needs to be implemented. Direct liquid cooling also known

as immersion cooling and classified into two major categories, single phase immersion cooling and two-phase immersion cooling [1].

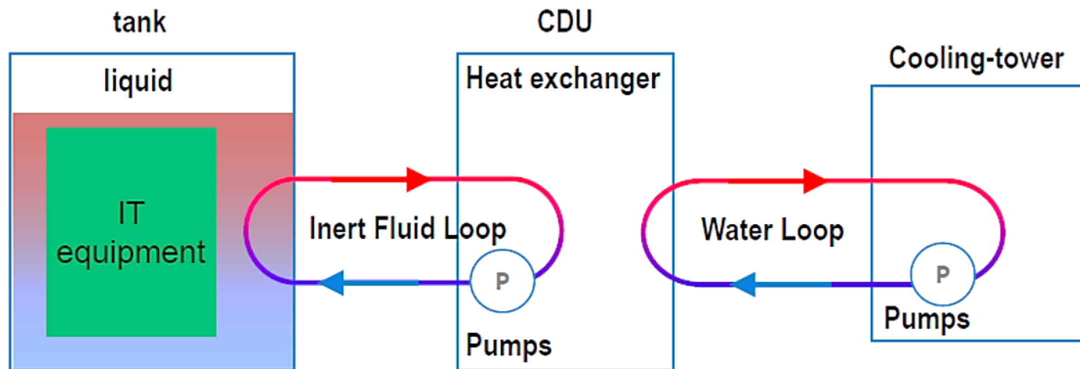

Figure 9: cooling loops of single-phase immersion cooling[8]

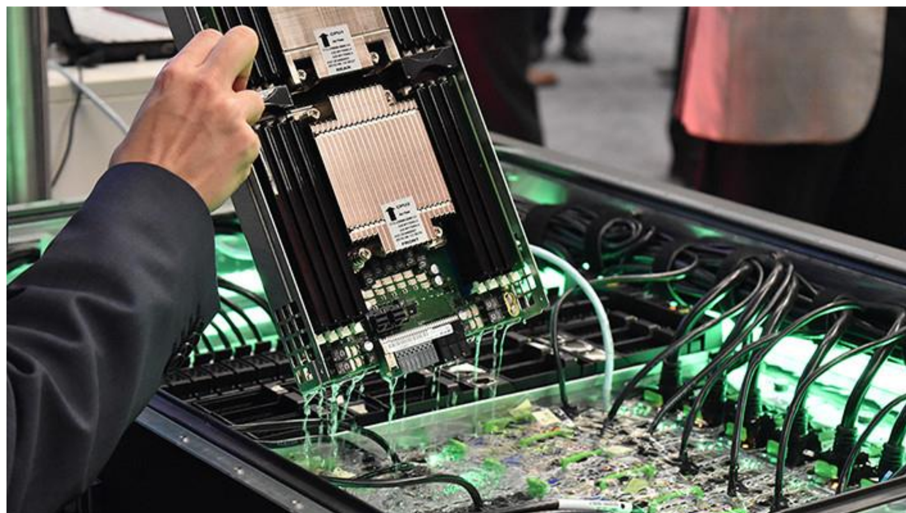

Figure 10: open bath of single-phase cooling[8]

In immersion cooling, high-energy electronic systems are immersed in dielectric liquid which has dielectric constant lower than water therefore they are safe for electronic systems. These liquids have higher thermal properties compare to air. Thus, they can help us to keep the systems below their temperature limit with lower velocities which reduce the friction and energy

consumption. Based on the boiling temperature and occurrence of phase change, immersion cooling can be divided in two categories of single and two-phase, which in single-phase, the coolant stays in liquid form but in two-phase, the liquid can boil in contact with the hot surface of electronic devices however this concept is not new and it is being used in many industries[9]. The high latent heat of vaporization helps heat to be extracted rapidly while the temperature of coolant stays almost constant.

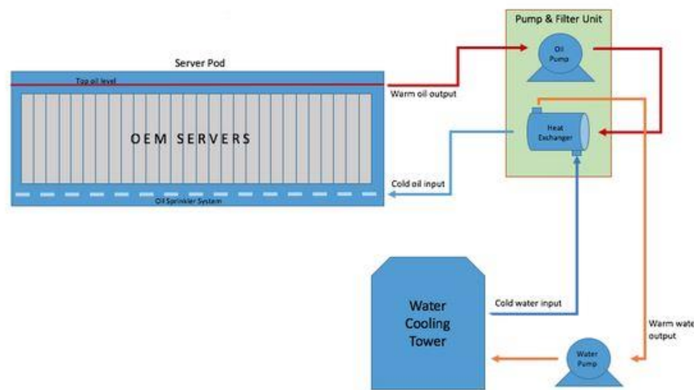

Figure 11: Schematic diagram for single phase immersion cooling [10]

In single phase immersion cooling, electronic systems are immersed into the dielectric coolant. Coolant carries heat and being circulated through heat exchanger. From heat exchanger, heat is ultimately rejected to ambient with cooling tower. For single phase research, many scientists used fluorocarbon fluid or oil as a coolant in their systems.

Traditionally, different thermal management strategies have been used in the field of cooling of electronics equipment. These strategies can be classified based on how efficiently they can transfer heat from the equipment. Figure 12 shows us the efficiency of each cooling method and data was explained as temperature difference of the equipment surface versus equipment heat flux. This figure shows that air natural cooling can handle very low amount of heat and based on the maximum temperature criteria for electronic cooling, the maximum heat density of equipment could be 0.05 W/cm^2. With forced convection of air cooling, it can go up to 0.2 W/cm^2. With natural convection of liquid immersion cooling, the power density can increase close to 10 W/cm^2. This happens due to better thermal properties of liquid like larger density and heat capacity. For higher power densities, the heat removal should be done through boiling. Boiling can increase the power density to more than 10. Although it should have mentioned here that, increasing performance of cooling with this method needs a very good surface enhancement which many scholars have been working on[11]–[13], [13]–[17].

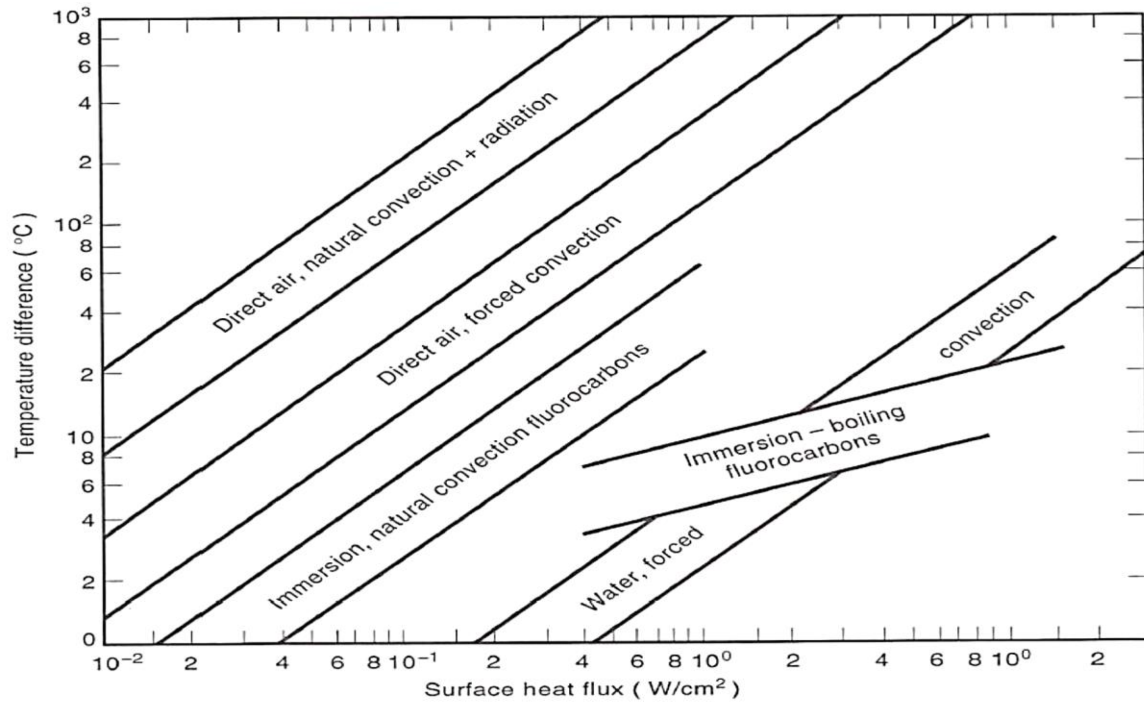

Figure 12: Efficiency of the different cooling methods[18]

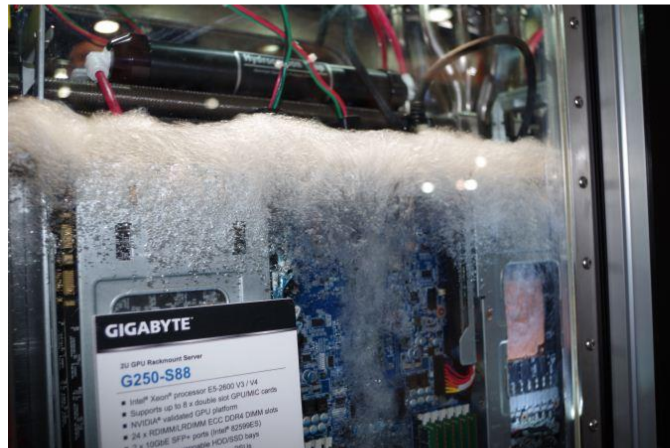

Figure 13: two immersion cooling of a GIGABYTE computer[19]

For the high power densities, the best method of cooling is the two phase immersion cooling in an open bath. Figure 13 shows the two phase immersion cooling of a GIGABYTE computer in simple tank. One of the benefits of open bath immersion cooling is the simplicity of the method. In this method, we have

an open bath which the server blades are placed in and the condenser is placed on top of the blades which cools down the vapor. In the tank, there is no need for any pumps for circulation of the liquid because gravity helps vapor goes up and the condensed liquid comes back to the tank. Because the vapor of the coolant is heavier than air so the vapor cannot escape from the tank. This helps us to have a system without needing any hermetic connectors which are expensive. Figure 14 shows the schematic of the server blades and tank for open bath immersion cooling.

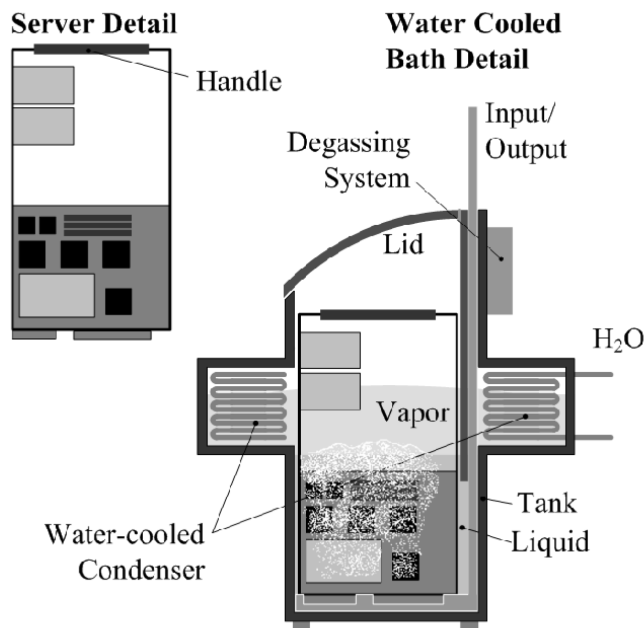

Figure 14: tank and server blades schematic for open bath immersion cooling

The cooling loop of the condenser uses water with an air cooler and there is no need for cooling compressors or chillers. This can save huge amount of money needed for investment and operation. This feature is due to boiling temperature of the liquid. Because the boiling temperature of the liquid is lower than the

maximum operation temperature and it is above the ambient temperature even in hot days of summer therefore, there is no need for chillers and this decrease the PUE of the data center close to 1. Figure 15 shows the schematic of the condenser cooling cycle of the open bath immersion cooling.

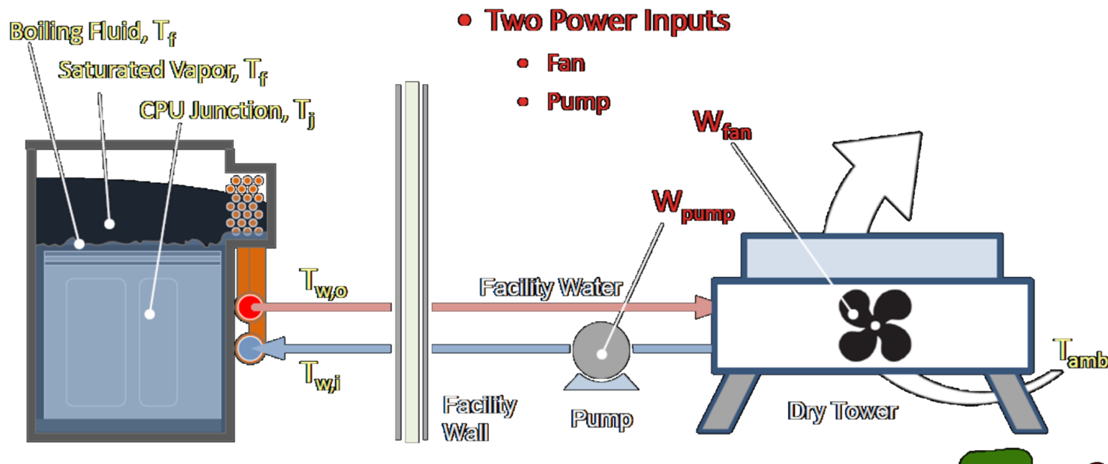

Figure 15: Schematic of two-phase open bath immersion cooling

Materials used as coolant categorized in FluoroCarbons (FC) and Hydrofluoroether (HFE) which are a class of organic solvers and They are typically colorless, odorless, tasteless, low toxicity, low viscosity, and liquid at room temperature. The boiling point of HFEs vary from 50 °C to nearly 100 °C.

Table 1 and

Table 2 show the liquids are normally used as coolant for immersion cooling for both single and two-phase. The selection of coolant should be based on the boiling temperature of the liquids. For the single phase cooling, the boiling

temperature must be over the maximum temperature of the surfaces and we must be sure that the amount of heat cannot convert the liquid phase to vapor phase. Most of the thermal properties are similar therefore the other criteria of choosing the liquid is the compatibility of the liquid with the equipment and the effect of the liquid on the environment in the long term.

Table 1: Properties of the liquid used in immersion cooling [20]

		HFE7300	HFE7500	HFE7700	FC-72
Boiling Point	C	98	128	167	56
Critical Pressure	MPa	1.88	1.55	1.41	1.83
Vapor Pressure	kPa	5.9	2.1	<0.1	30.9
Heat of Vaporization	kJ/kg	102	89	83	88
Liquid Density	kg/m3	1660	1614	1797	1680
Kinematic Viscosity	cSt	0.71	0.77	2.52	0.38
Absolute Viscosity	cP	1.18	1.24	4.54	0.64
Specific heat	J/kg-K	1140	1128	1040	1100
Surface Tension	mN/m	15.0	16.2	18	10
Dielectric Strength Range, 0.1" gap	kv	>25	>25	>25	38

Table 2: Properties of the liquid used in immersion cooling [20]

		HFE7000	Novec649	HFE7100	HFE7200
Boiling Point	C	34	49	61	76
Critical Pressure	MPa	2.48	1.88	2.23	2.01
Vapor Pressure	kPa	65	40	27	16
Heat of Vaporization	kJ/kg	142	88	112	119
Liquid Density	kg/m3	1400	1600	1510	1420
Kinematic Viscosity	cSt	0.32	0.40	0.38	0.41
Absolute Viscosity	cP	0.45	0.64	0.58	0.58
Specific heat	J/kg-K	1300	1103	1183	1220
Surface Tension	mN/m	12.4	10.8	13.6	13.6
Dielectric Strength Range, 0.1" gap	kv	>25	>40	>25	>25

Chapter 2 : Two-phase immersion cooling

In this section, two-phase cooling of electronic equipment will be discussed. Current research is based on the numerical and experimental research on two-phase cooling.

2.1. Literature review

Due to high importance of boiling in engineering applications, many researchers have been doing research on this topic and vast investigations were performed regarding thermal performance and associated heat transfer phenomena in boiling. Nukiyama [21] studied the various regimes and stages of pool boiling extensively. His experiments were studied by applying constant heat on the platinum, nickel, nichrome, iron wires which their electrical resistances were known through implementing a constant current. With this

method they could measure a constant heat flux using a Wheatstone bridge which helped them to find the temperature of the wires while boiling.

Figure 16 provides the pool boiling curve that was pieced together from the experiments. The first regime up to zone A is the natural convection regime, in which the surface temperature is below the saturation temperature of the liquid in the pool. The density difference between the hot fluid close to the surface and the cold fluid far away from the surface creates fluid motion in the pool.

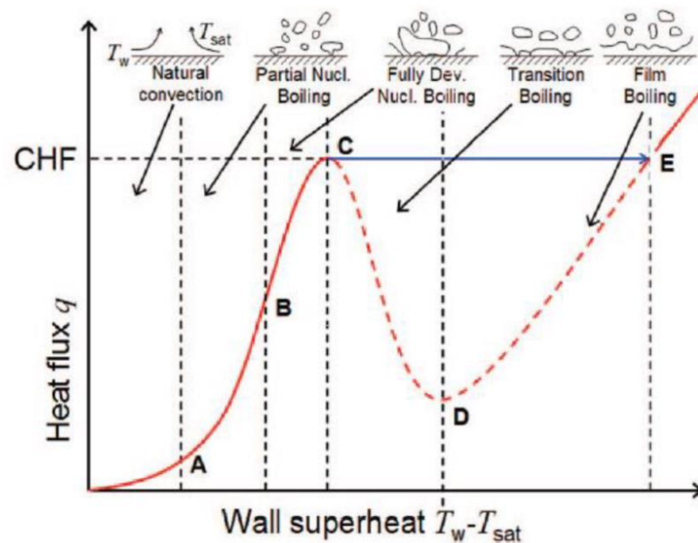

Figure 16: characteristic curve of boiling [21](heat flux vs wall superheat temperature)

The curve is approximately linear in this regime and the slope of this curve provides the heat transfer coefficient. As the heat flux increases, the nucleation activity is initiated, and this point is called onset of nucleate boiling (ONB). The heat flux required to initiate the boiling activity is called incipience heat flux. The transition in the heat transfer mechanism from single-phase natural convection

to partial boiling is marked by decrease in surface temperature, since for the same heat flux value, boiling has more heat transfer rate than single-phase natural convection. This overshoot in temperature is observed only in increasing heat flux experiments, since the energy required to initiate nucleation is more than energy required to deactivate the nucleation activity. Between points A and B is the partial boiling regime in which heat transfer is due to both natural convection and boiling. The slope of the curve is now steeper, which means that compared to the convection regime a relatively large change in heat flux is required to increase the difference in surface temperature by an equivalent value. This increase in heat transfer rate is mainly due to the numerous nucleating bubbles removing the heat from the boiling surface and transferring it to the pool liquid. Between the points B and C is the fully developed boiling regime in which the boiling effects are highly dominant over the convective effects and the entire surface is nucleating.

The system in which the electronic packages are immersed in a pool of dielectric fluid maintained at a specified temperature is generally referred to a pool boiling system. The temperature of the fluid can be maintained at its saturation temperature or at a subcooled temperature. Using the same experimental setup discussed in this study Gess et al. [22] performed pool boiling investigations for three different surfaces – bare silicon, microporous and microfinned. The thermal performance between FC-72 and Novec 649 fluids were compared and the different subcooling values for these dielectric

fluids were also tested. Heat flux values of up to approximately 14 W/cm² were achieved for the microfinned surface at the highest subcooling used in the study. Thiagarajan et al. [12] investigated the performance of cooling in pool boiling experimental test with microporous and plain surfaces in a different orientation like horizontal orientation, using Novec 7100 as coolant liquid. Two cases with different roughness values of the surface and three surfaces with microporous feature with different coating thickness values were investigated in this study. The results reveal increase in CHF values up to 60% for the microporous surface with low thickness coating, compare to the plain surfaces.

Recent studies on pool boiling like investigation by Jaikumar and Kandlikar [11], which the surfaces of open microchannels with porous fin were applied to reach 270% improvement in critical heat flux compared to the plain surface. Surfaces of copper block with the dimension of 20 mm x 20 mm in a horizontal configuration microchannels of size 10 mm x 10 mm was machined in the central of the surface were used in this pool boiling study. They used FC-87 as the coolant for this research. Five different combination of channel dimensions (width and depth) were investigated to specify the influence of the channel configuration on boiling performance of the channels. The ratio of width to depth of that channel was found to be a vital parameter, and the best performance recorded in this investigation was for a ratio of one. CHF values in the vicinity of 65 W/cm² were mentioned by El-Genk [24], for facing copper microporous

surfaces on upward configuration of 10 mm by 10 mm heater at 30° C subcooled temperature of the Performance Fluid 5060 liquid. The next parameters which were tested on the pool boiling configuration involving surface characteristics, coolant liquid, subcooled temperature and surface normal angle. Using similar surface enhancements but in a more conventional pool boiling setting, Sridhar [48] achieved heat flux values of up to 47 W/cm² with the micro-finned heat sinks. The change in thermal performance of a chip due to the presence of neighboring dies in a multi-chip module was also investigated in this study. The pool boiling studies by Ramakrishnan [23] using Novec 649 and HFE-7100 fluids also investigated the thermal performance of microporous and micro-finned heat sinks, and reported highest heat fluxes close to the 20 W/cm² for the microporous surfaces. This study also investigated the effect of fluid contamination by intentionally contaminating the working fluid with dioctyl phthalate. The results show that the microporous surface had the highest loss of performance with increase in superheats of up to 10°C. The microfinned heat sink was recommended to be used in operations prone to fluid contamination, as the large feature size has higher resistance to contamination and also offers better performance than the bare silicon surface.

It must be noted that while the studies reviewed above show the effect of different parameters on the thermal performance of the pool boiling system, a direct comparison between these studies cannot be made due to the large differences in the volume of the pool. While the studies by Sridhar [25] use a

large pool that is similar to OBI approach, the studies by Gess [22] use a relatively smaller pool. Therefore, the highest heat flux values alone cannot be used to quantify the performance of the system. Nevertheless, it can be observed that for any pool boiling system, employing tailored surfaces and increasing the degree of subcooling will result in higher heat dissipation compared to a system with a plain surface and a saturated pool.

2.2. Numerical analyses

To simulate subcooled boiling, the Non-equilibrium model is used. Subcooled boiling is a kind of boiling that the bulk fluid temperature is less or equal to the boiling temperature, but the wall temperature is high enough to make boiling to happen. At first, the liquid gains energy to reach the boiling condition and after that the liquid starts to change phase however the temperature of liquid stays fixed but the temperature of vapor can be changed due to energy transfer from the wall. Since boiling is a very complicated phenomenon, the energy also can be transferred between phase like transferring energy from the high temperature vapor to the liquid [26]. This can change the vapor quality and temperature in the area even far from the wall too.

The first equation that needs to be solved is continuity equation. All equations for RPI method need to be solved separately for each phase [27].

$$\frac{\partial}{\partial t}(\alpha_i \rho_i) + \nabla.(\alpha_i \rho_i \vec{v}_i) = \sum_{j=1}^{n} \dot{m}_{ij} - \dot{m}_{ji} \quad (1)$$

Where α is the mass fraction of each phase, ρ is the density of that phase that can be function of temperature and pressure and, j and i show the phase

of fluid, liquid or vapor. $\vec{v}_i$ represents the velocity of that phase and $\dot{m}_{ij}$ depicts the mass transfer from phase i to j and $\dot{m}_{ji}$ depicts the mass transfer from phase j to i.

The momentum equation for boiling flow is defined as

$$\frac{\partial}{\partial t}(\alpha_i\rho_i\vec{v}_i) + \nabla.(\alpha_i\rho_i\vec{v}_i\vec{v}_i) = \alpha_i\nabla \mathrm{p} + \nabla.\bar{\bar{\tau}}_i + \alpha_i\rho_i g + \sum_{j=1}^{n}\vec{R}_{ij} + \dot{m}_{ij}\vec{v}_{ij} - \dot{m}_{ji}\vec{v}_{ji} + \vec{F}_i \quad (2)$$

Where $\vec{R}_{ij}$ shows the force of interaction between phases and $\vec{F}_i$ represents the forces includes external body force, lift force, wall lubrication force, virtual mass force and turbulent dispersion force. In addition, p is the pressure, $\bar{\bar{\tau}}_i$ is phase stress-strain tensor and g are the gravity.

For the reason that the boiling is a phase change phenomenon, the typical energy equation cannot be solved in this case. the formal energy equation includes heat capacity that is not meaningful while changing of phase happens therefore the energy equation should be solved based in the form of enthalpy. This form is capable of simulating the effect of changing phase. Accordingly, the energy equation for each phase can be written

$$\frac{\partial}{\partial t}(\alpha_i\rho_i h_i) + \nabla.(\alpha_i\rho_i\vec{v}_i h_i) = \alpha_i\frac{dp_i}{dt} + \bar{\bar{\tau}}_i:\nabla\vec{v}_i + \nabla.q_i + \sum_{j=1}^{n}Q_{ij} + \dot{m}_{ij}h_{ij} - \dot{m}_{j} \quad (3)$$

Where h_i is the enthalpy of i phase, q_i is the heat flux and Q_{ij} is the intensity of heat exchange between phase i and j. h_{ij} characterizes the enthalpy transfer from phase i to j and h_{ji} characterizes the enthalpy transfer from phase j to i.

Generally boiling is turbulent phenomena and to simulate it the turbulent equation should be solved along other equations. the most suitable turbulent model for industrial cases is Reynolds Averaging Navier-Stocks model (RANS)[28], [29]. Amongst RANS models, $k-\omega$ model has good precision and stability. Therefore, for the present work, this model was selected. The basic idea of this model is to find the distribution of turbulence kinetic energy (k) and specific rate of dissipation (ω) in the domain through solving transport equation of each parameter.

$$\frac{\partial}{\partial t}(\alpha_i \rho_i k_i) + \nabla.(\alpha_i \rho_i \vec{v}_i k_i) = \nabla.\left(\alpha_i \mu_{eff} \nabla k_i\right) + S_i^k \tag{4}$$

$$\frac{\partial}{\partial t}(\alpha_i \rho_i \omega_i) + \nabla.(\alpha_i \rho_i \vec{v}_i \omega_i) = \nabla.\left(\alpha_i \mu_{eff} \nabla \omega_i\right) + S_i^\omega \tag{5}$$

Where μ_{eff} represents the effective viscosity, which is calculated based on the vapor quality and the empirical correlations. S_i^k and S_i^ω shows the source term of k equation which includes the production of turbulence kinetic energy, interphase turbulent momentum transfer for each phase and so on.

The concept of RPI is based on the dividing the total wall heat flux to three main parts, the convective heat flux, the quenching heat flux and the evaporative heat flux.

$$\dot{q}_W = \dot{q}_C + \dot{q}_Q + \dot{q}_E \quad (6)$$

The convective heat flux $\dot{q}_C$ is defined as

$$\dot{q}_c = h_C(T_w - T_l)(1 - A_b) \quad (7)$$

Where A_b is expressed as area of influence where occupied by nucleating bubbles, thus $(1 - A_b)$ is the portion of wall surface which is not covered by fluid. h_C represents single phase heat transfer coefficient, and T_w and T_l show the wall and liquid temperature respectively.

The definition of are influence is

$$A_b = \min\left(1, K\frac{N_w \pi D_w^2}{4}\right) \quad (8)$$

Where N_w is nucleate site density, K is the empirical constant and usually is assumed to be 4[30]. The D_w is departure diameter of bubbles from the surface. This form of Area of Influence equation helps to avoid numerical instabilities

which occurs caused by unbound empirical correlations of nucleate site density equation[30]. The K can be calculated by

$$K = 4.8e^{\left(-\frac{Ja_{sub}}{80}\right)} \tag{9}$$

Where Ja_{sub} is subcooled Jacob number and is defined as

$$Ja_{sub} = \frac{\rho_l C_{p_l} \Delta T_{sub}}{\rho_v h_{fv}} \tag{10}$$

Where ρ_l is density of sub-cooled liquid, ρ_v is vapor density, C_{p_l} is sub-cooled liquid specific heat capacity.

The quenching heat flux ($\dot{q}_Q$) is defined as energy transfer when the liquid fills the wall vicinity after detachment of the bubble, and it is calculated by

$$\dot{q}_Q = \frac{2k_l}{\sqrt{\pi \lambda_l T}} (T_w - T_l) \tag{11}$$

Where λ_l is the diffusivity and T is the periodic time. λ_l is expressed as

$$\lambda_l = \frac{k_l}{\rho_l C_{p_l}} \tag{12}$$

The last flux term in the RPI model is called evaporative flux ($\dot{q}_E$) and it is expressed by

$$\dot{q}_E = N_w V_d \rho_v h_{fv} \tag{13}$$

Where N_w represent nucleation site density, V_d is the volume of the bubble, ρ_v is the density of vapor and h_{fv} represents the latent heat of the fluid.

Nucleate site density is one of the most important parameter in the simulation of boiling and for the present study, Kocamustafaogullari and Ishii [31] model is used for prediction of nucleate site density, which includes an empirical correlation which is given by

$$N_w^* = f(\rho^*) r_c^{*-4.4} \tag{14}$$

In this empirical formula, the parameters are defined as

$$N_w^* = N_w D_w^2 \tag{15}$$

$$r_c^* = 2r_c / D_w \tag{16}$$

$$\rho^* = (\rho_l - \rho_v)/\rho_v \tag{17}$$

Where D_w is wall departure diameter and r_c is given by

$$r_c = \frac{2\sigma T_{sat}}{\rho_v h_{fv} \Delta T_w} \tag{18}$$

In this formula, the σ represents surface tension, T_{sat} shows the saturation temperature of the fluid which can be function of pressure if the pressure change in the case is not negligible. ΔT_w depicts the difference between the wall temperature and the fluid temperature. Finally, the function $f(\rho^*)$ is given

$$f(\rho^*) = 2.157 \times 10^{-7} \rho^{*^{-3.2}} (1 + 0.0049\rho^*)^{4.13} \tag{19}$$

by

In most boiling cases, an empirical model is used to calculate bubble departure dimeter like Kocamustafaogullari and Ishii[32] or Unal[33] but in this case, research shows that the bubble departure diameter is now function of wall temperature difference and surface tension and as long as the boiling regime is nucleate boiling, the bubble departure diameter is constant and equal to 0.1mm [34].

2.3. Simulation setup and boundary conditions

For this study, the FC-72 was chosen which has latent heat vaporization about 88 J/g while the boiling happens at atmospheric pressure and boiling temperature of 56°C. The increase in working pressure is not recommended due to increase of boiling temperature which can damage the electronic

components. Table 3 shows the properties of FC-72 for the two phases of liquid and vapor.

Figure 17 and Figure 20 show the boundary conditions for the validation case and the test case. These cases include one or two processors which are modeled by a uniform heat flux boundary condition. for the test cases, the heater is simulated to the wall by 2 mm space to consider the real thickness of processors. The size of processor for the validation test is 9mm by 9mm and the container is 200mm x 200mm x 500mm. for the test case, the processor size is 40mm x 40mm and the container dimension is 320mm x 200mm x 50mm. the space between the two processor for the double chips case is 40mm. all sides of containers, except one, is assumed to be closed wall and to be in insulated thus the zero-heat flux was used as boundary conditions. The top side of each container was assumed to be open and the pressure outlet boundary condition was chosen which let the flow enters and exits from the boundary. This condition allows the vapor, or the liquid leaves the container due to the buoyancy and allows the liquid comes back to the domain. In the real case, the vapor goes up and by contacting a condenser, it gets cooled and the saturated or subcooled liquid comes back to the domain but for the simulation, because of limitation in boiling model and computational resources, it is substituted by the opening boundary condition. The exit flow satisfies zero-gradient condition and for the inlet flow, the pressure is ambient pressure, but the temperature was set based on the temperature difference with saturation

temperature which helps us to simulate the subcooled boiling in our case where it was set as one degree difference.

Table 3: Thermal properties of FC-72 at boiling temperature [13]

	Properties	**Value**
	Average Molecular Weight	338
	Boiling Point (1 atm)	56°C
	Latent Heat of Vaporization	88 J/g
liquid	Liquid Density	1680 kg/m^3
	Kinematic Viscosity	0.38 centistokes
	Absolute Viscosity	0.64 centipoise
	Liquid Specific Heat	1100 $J\ kg^{-1}\ C^{-1}$
	Liquid Thermal Conductivity	0.057 $W\ m^{-1}\ °C^{-1}$
Vapor	vapor Density	13.1 kg/m^3
	Kinematic Viscosity	0.1 centistokes
	Absolute Viscosity	0.124 centipoise
	Vapor Specific Heat	900 $J\ kg^{-1}\ C^{-1}$
	Vapor Thermal Conductivity	0.0235 $W\ m^{-1}\ °C^{-1}$

2.4. Result and Discussion

2.4.1 Validation case

To validate wall boiling model, an experimental case with simple geometry is chosen and the result of numerical simulation is compared to the experimental result to see the performance of the model. Therefore, an experimental with FC-72 as liquid is selected[35]. The experimental includes a chamber with a single chip at the bottom of the chamber to find the boiling characteristic curve. The size of chip is 9x9 mm and the surroundings of the chip is kept far from the chip to make sure that the other walls cannot affect the results. Figure 17 shows the geometry of chamber used for numerical simulation and validation case.

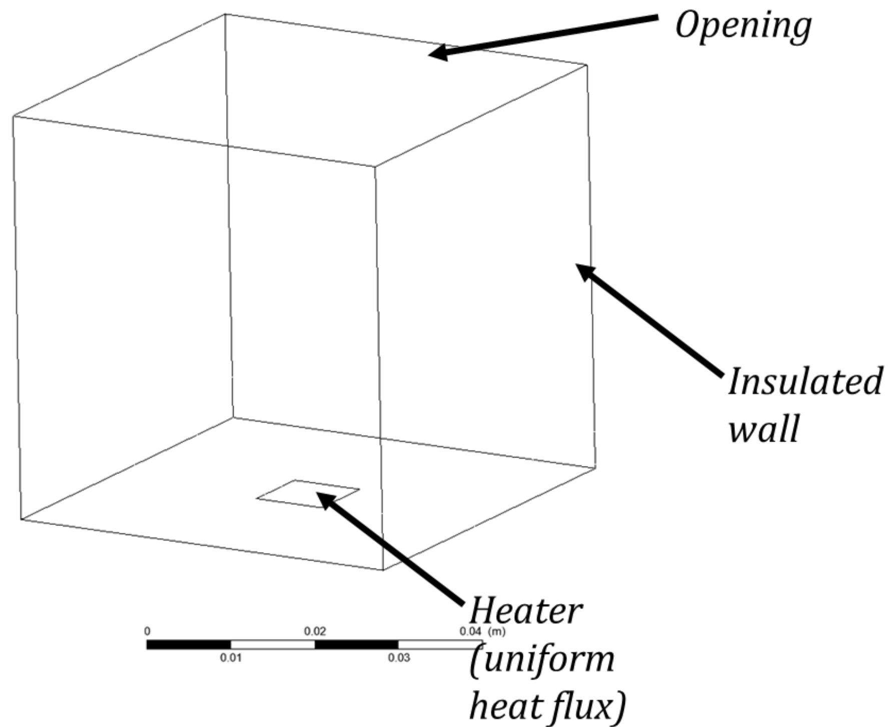

Figure 17: the chamber geometry for validation case and boundary conditions

For this study, FC-72 properties are used. FC-72 is one of the fluorocarbons which is widely used in experiments and industrial cases for the purpose of the two-phase cooling. shows the properties of FC-72 at the temperature of 55°C and atmospheric pressure. For the vapor, properties are function of temperature and pressure due to lack of data for the vapor properties, a nonlinear equation of state is used for calculation and the calculated properties later was imported as table to the software for simulation.

This geometry was simulated for 3 different grid numbers to be sure that the numerical error due to spatial discretization is minimum and the error of

simulation reaches to less than 1 percent and the convergence criteria was set to $1e^{-6}$. To increase the stability of solution, all relaxation factor was set to 0.1 and the multigrid method is used.

Figure 18 shows the isosurface of 10% vapor volume fraction colored by the velocity of vapor phase. As it shows, the bubble start to rise from the surface of the heat source and goes up due to gravity forces. Because of the natural convection flow inside the chamber, the bubbles tend to gather in the midline of the chamber. Figure 19 shows the saturation boiling curve of validation case. this curve shows that as heat flux increases the difference between wall temperature and saturation temperature also increases. The current simulation just covers the nucleation boiling regime which is up to 15 W/cm^2.

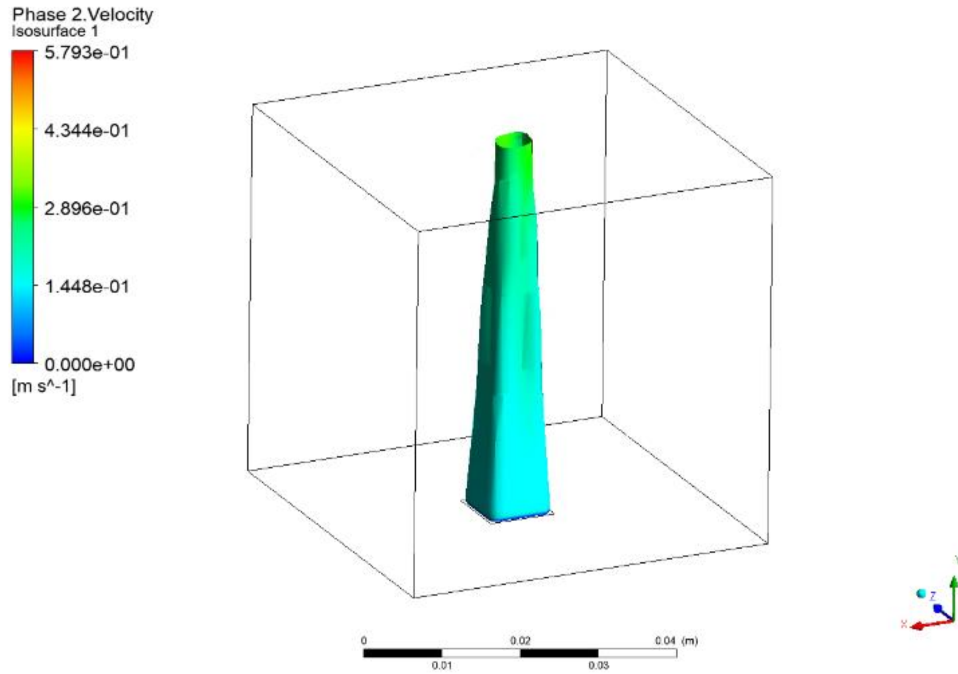

Figure 18: Isosurface of 10% vapor volume fraction colored by the velocity

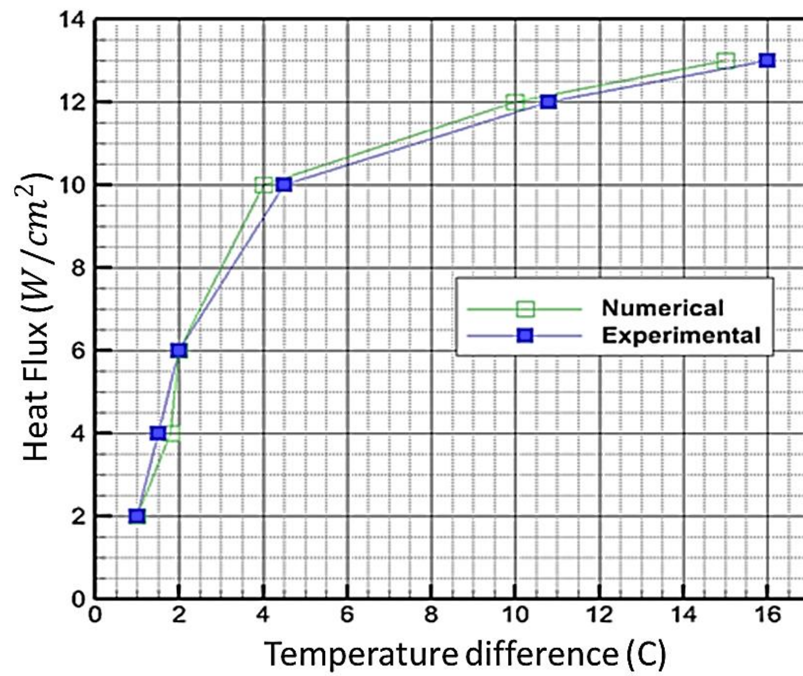

Figure 19: saturation boiling curve of FC-72 for validation case

2.4.2 Single and double CPUs

In this research, two-phase immersion cooling for single and double chipset are studied for FC-72 as coolant. The ambient temperature and temperature of liquid are kept at 56°C which is the boiling temperature of the FC-72. The chipset size for all cases are 4cmx4cm that is close to all CPU sizes. The cases are simulated for different inclination and for a variety of power. In this case the pressure is kept at atmospheric pressure. The properties which are used for simulation are depicted inTable 3.

Figure 20 describes the boundary condition used for this simulation. Figure 21 depicts the isosurface of 10% volume fraction of vapor over two chipsets. As it shows, the boundary layer starts from the bottom chipsets and it tends to the center line of the chipset and it covers the center area of top chipsets. The top chipset also has boiling boundary layer therefore, the boundary layer starts to grow from both sides of the top chipset.

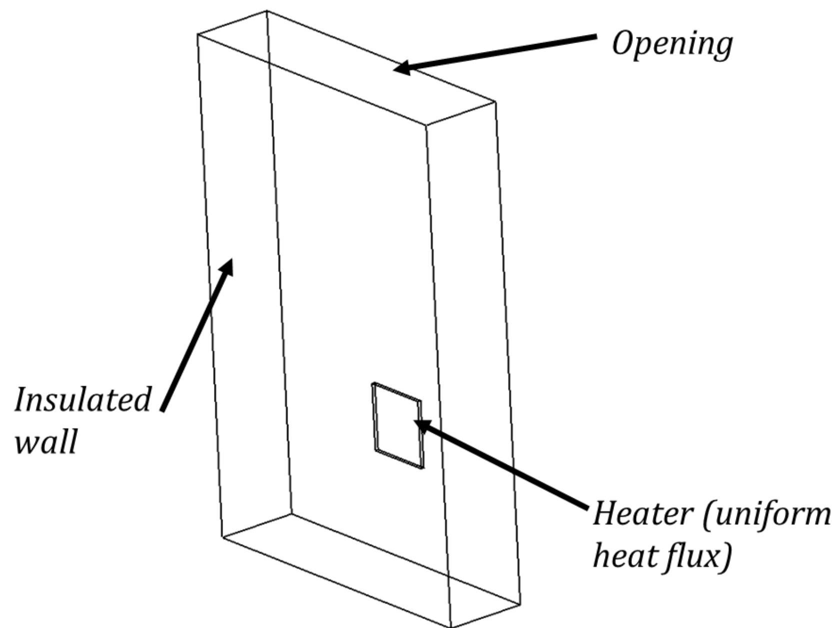

Figure 20: Domain geometry and Boundary conditions

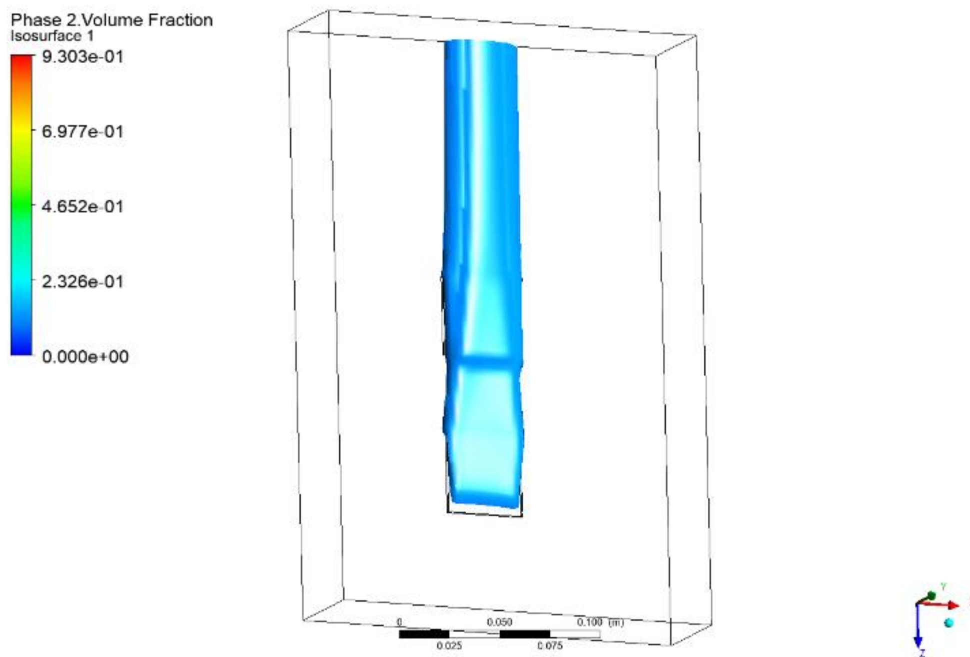

Figure 21: Isosurface of vapor volume fraction over chipsets

Figure 22 shows the distribution of vapor volume fraction over the chipsets. The bottom figure shows the case which the power of chipset is 4 W/cm^2. In this case most of area of the bottom chipset is covered by the liquid and at the top of the bottom chipset it starts boiling but for the top chipset, it is covered by the vapor except two narrow band at the left and right of the chipset which has contact with liquid. the top figure shows the case which the power is 15 W/cm^2. For this case, the boiling starts from the middle chipset and the quality of vapor will reach about 0.25. the top chipset is fully covered by the vapor and on the top of this chipset the quality of the vapor reaches about the 0.93.

Figure 23 shows the effect of inclinations on the boiling curve. The general pattern for all curves is the same but the curve is shifted to the left which is the effect of inclination. It shows that by changing the inclination, the temperature difference reduces due to penetration of liquid over the chipset surfaces. Also, the curves are diverging for higher heat fluxes and as heat flux increases, the temperature difference also increases.

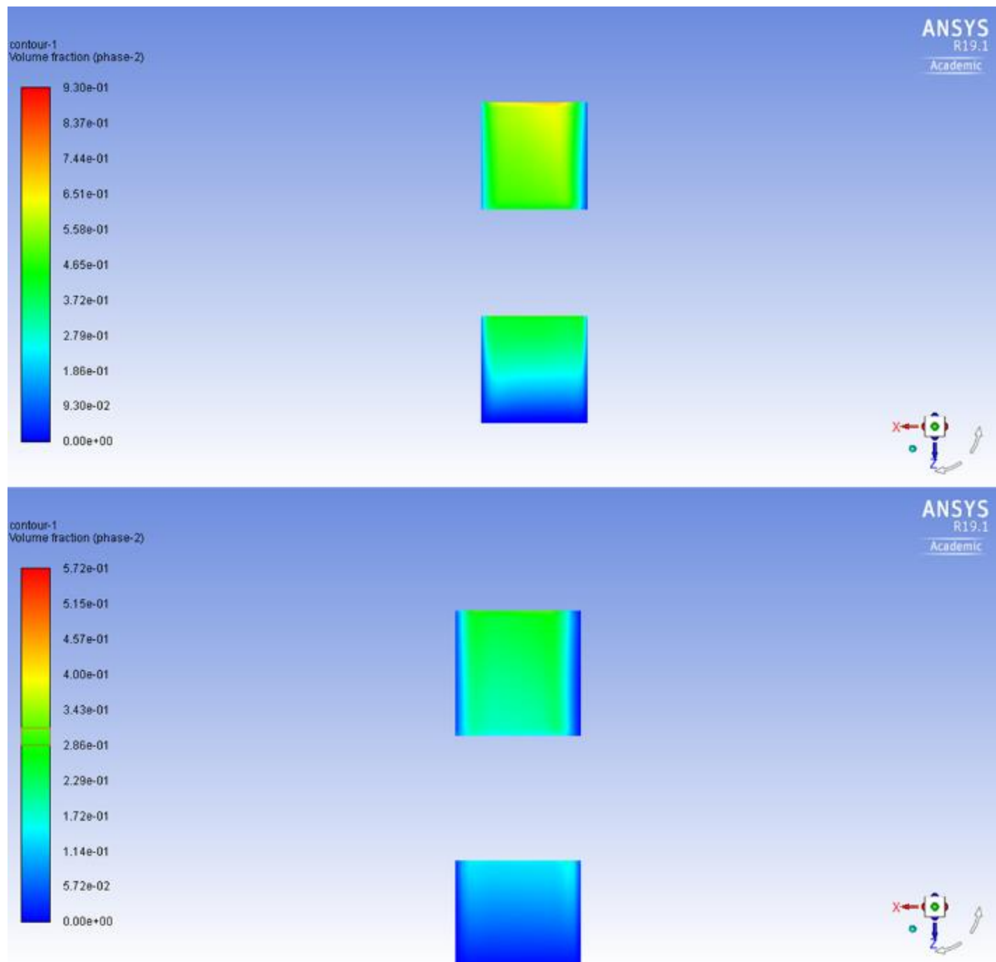

Figure 22:distribution of volume fraction over the chipsets (bottom:4W/cm^2, top:15W/cm^2).

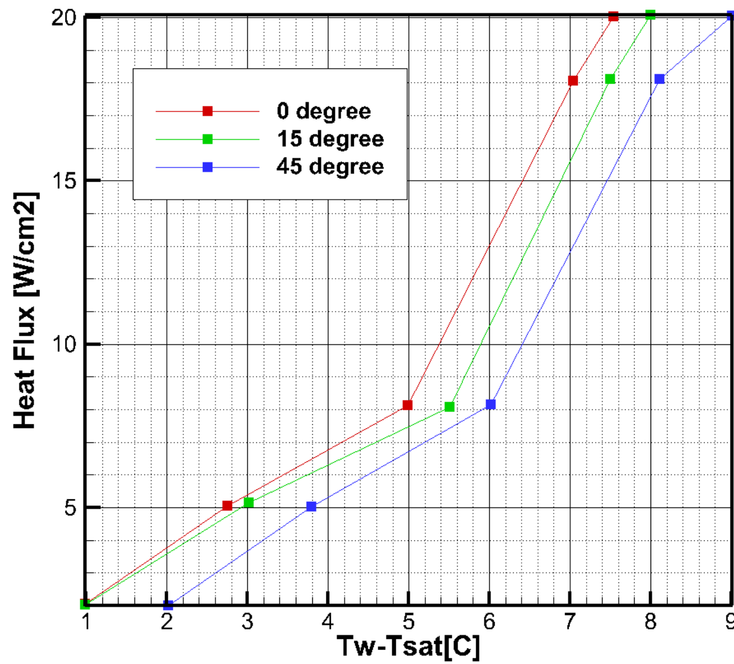

Figure 23: Effects of different inclinations on simulated boiling curves of the bottom chipsets

2.4.3 Single Die

In this part of this research, the performance of a single die in the pool boiling condition was considered. The size of the die is 10mm by 10mm and the depth of the tank was assumed as 50mm. the Hight of the tank was assumed 100mm to reduce the effect of the boundary on the results. All walls were considered as insulated and the die has the constant heat flux condition. the temperature of the was calculated based on the area averaging method. The top surface is

outlet and the boundary condition can allow the vapor to leave the tank and the liquid fraction is calculated based on the mass and this mass can come back to the tank.

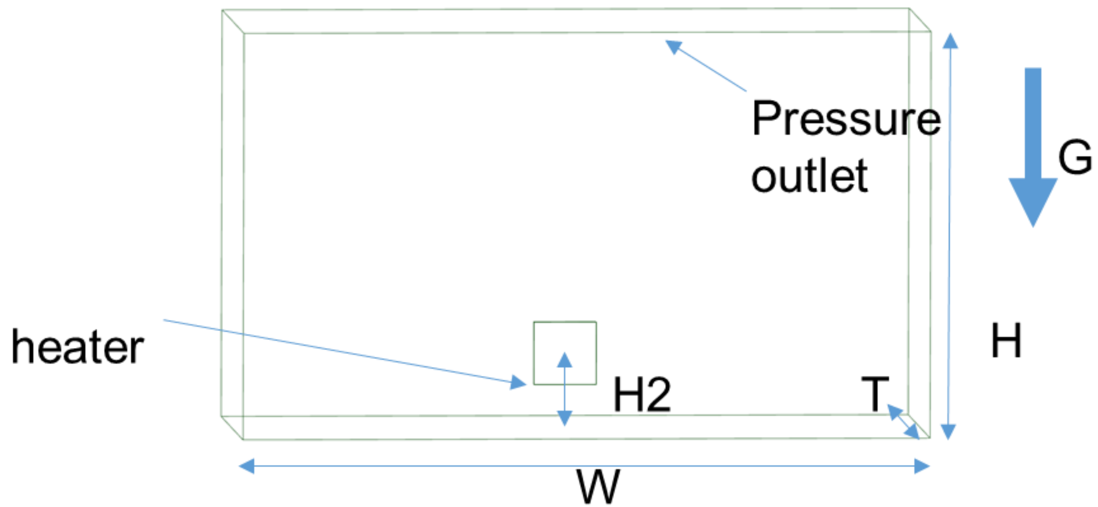

Figure 24: configuration and boundary condition of a single die in vertical condition

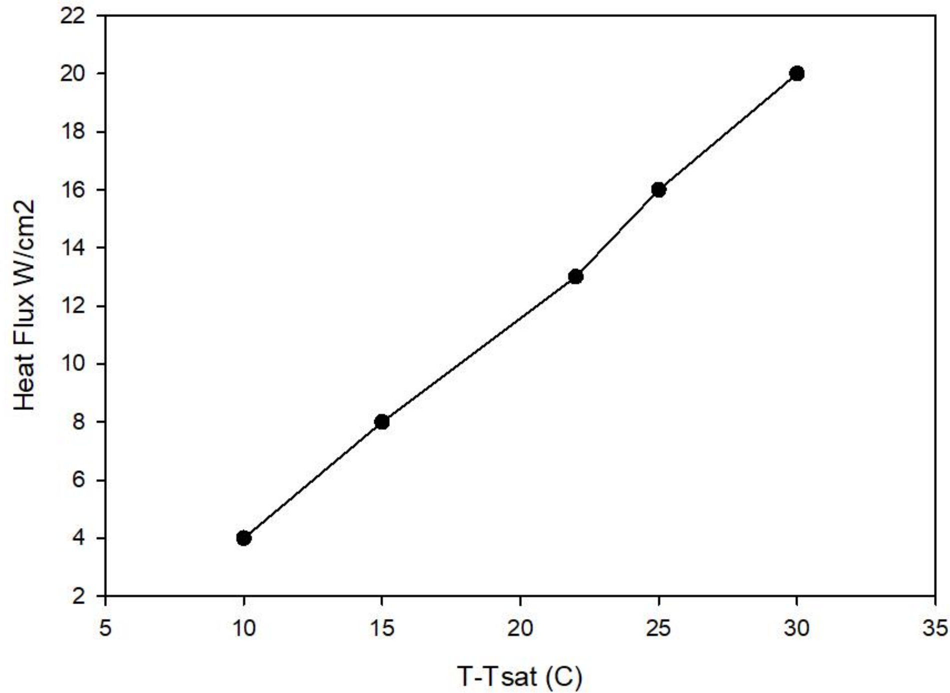

Figure 25: results of single die 10x10mm with vertical condition

Figure 24 shows the domain and boundaries of the simulation. Figure 25 shows the results of the simulation, for the 4 W/cm^2, the wall superheat temperature is 10° C. as the power density increases to 20 W/cm^2, the wall superheat temperature increases to 30° C. one of the weakness of the numerical simulation is that the model does not have any sense of critical heat flux of the pool boiling, therefore as we increase the power density, we get a solution but at that point the condition might pass the nucleate regime and enters to critical heat flux.

2.4.4 Side by side configuration of the die

In this section, the effect of the horizontal space between to die was studied. The purpose of this study is to reveal whether the horizontal space influences the performance of cooling or not. Figure 26 shows the boundary condition and computational domain. To reduce the computational time, the domain cut half and a symmetry condition were substituted for that cut plane to simulate the effect of the second die. The size of die is 10mm by 10mm and the distance between two dies was considered as 20mm and 30mm therefore, the space between the die and the symmetry plane was considered as 10mm and 15mm. the depth of the tank was considered as 50mm and the height of the tank was considered as 100mm. the die was placed 20mm above the bottom of the tank and the top of the tank was considered as pressure outlet. This condition let the vapor passes through the boundary and the saturated liquid can be replaced based on the mass conservation. This way the mass inside the domain is conserved and the convergence of continuity equation is guaranteed.

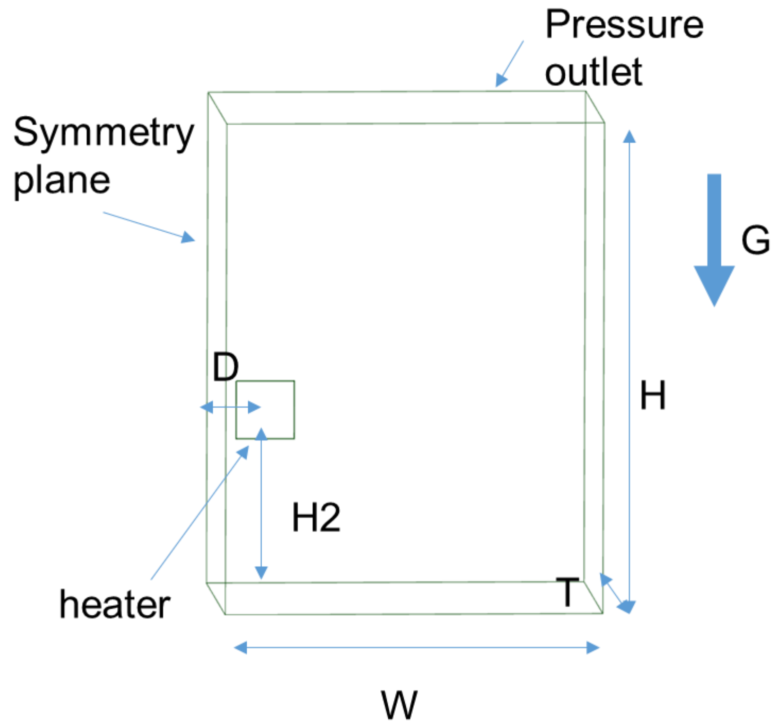

Figure 26: side by side configuration simulation using symmetry boundary condition

The case was simulated for different power which varies from 4 to 20 Watts and as the area of the die is 1 cm^2 therefore the power density of the die varies from 4 to 20 W/cm^2. Figure 26 shows the comparison of the results for the two different space of the die. Both cases show the similar behavior and this behavior is almost the same as single die in pool boiling. Therefore, we can conclude that the horizontal configuration has no effects on the performance of the die.

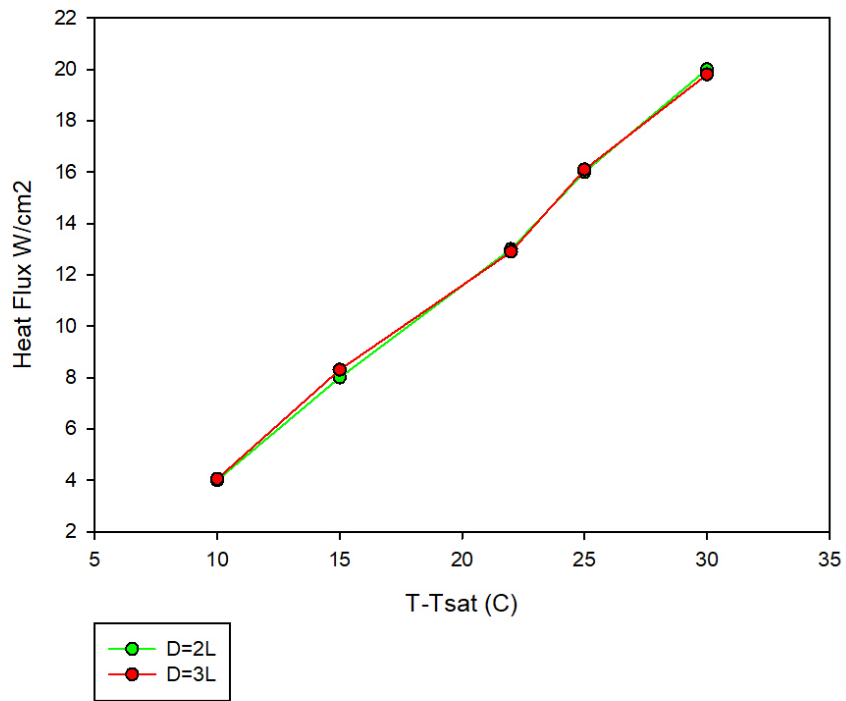

Figure 27: results of side by side configuration 10x10mm die

2.4.5 Vertical configuration

In this section, we examined the effect of the vertical space between the dies to check how temperature increases on the surface. For this study 4 different spaces were selected 10 to 40 mm for two die with dimension of the 10 mm by 10mm. the top surface of the domain was considered as the pressure outlet which lets the vapor passes and the liquid substitutes to maintain the continuity inside the domain. Except the dies, the rest of walls was considered as the insulated walls and the dies were considered as constant heat flux. Figure 28 shows the simulation domain of the vertical case.

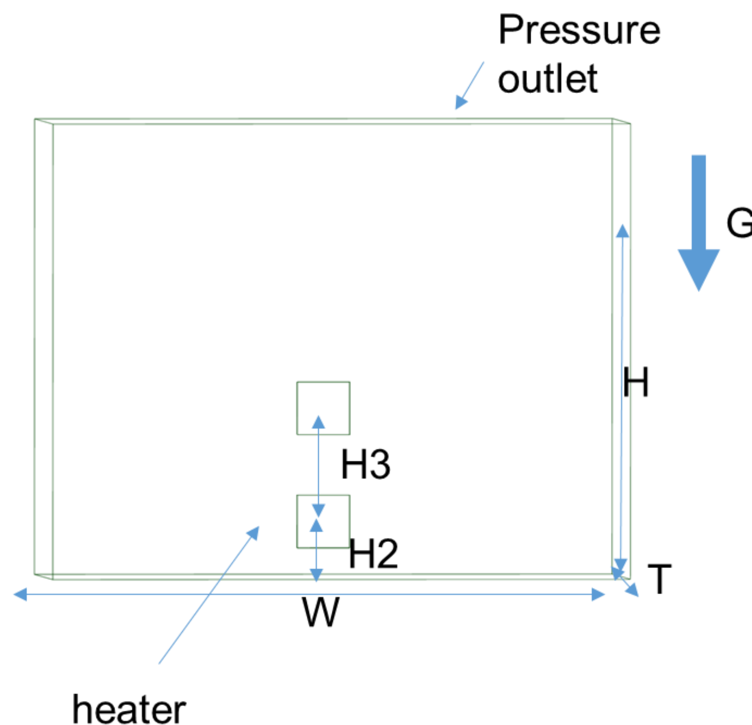

Figure 28: vertical configuration of two dies and boundary conditions

Figure 29 shows the results of the vertical space simulation. As the results show, for the 3L and 4L space the results are almost the same as the single heater which shows after 3L the heaters cannot influence each other. the 1L and 2L space can affect the upper surface.

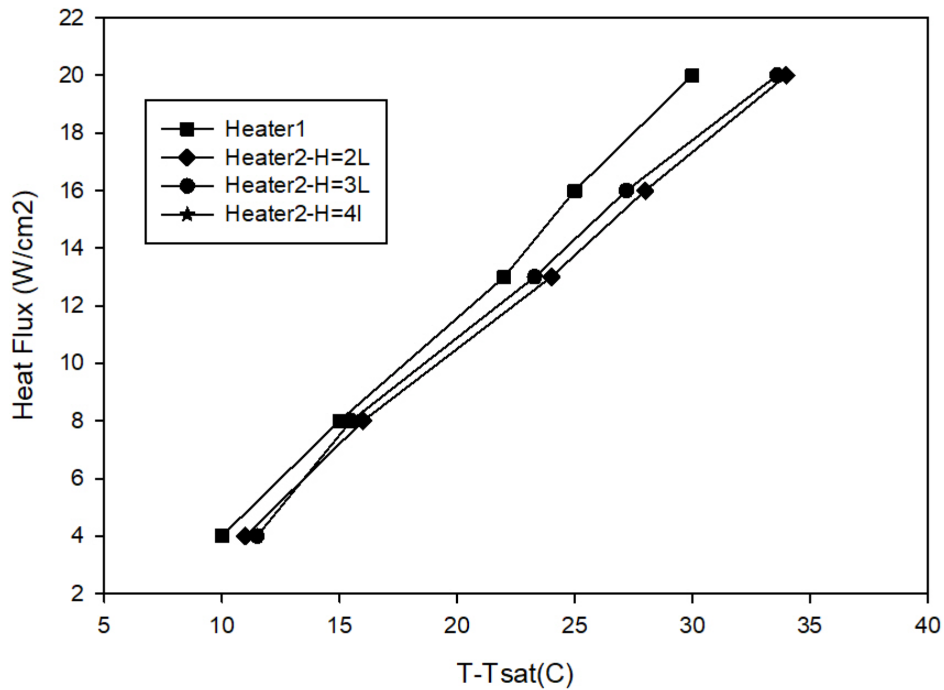

Figure 29: results of vertical configuration boiling

Chapter 3 Test cell design

To test the performance of open bath immersion cooling, a test cell is designed. Figure 30 shows the schematic of the designed test cell for the purpose of measuring cooling characteristic curve of the simulated electronics board. The test cell works in ambient pressure and the temperature of the bath is controlled by a hot plate at the bottom and surroundings of the tank is covered with 3d printed insulation pads to limit heat transfer to the outside of the system and prepare a uniform temperature inside the tank. A beaker is used as a tank which allows us to check the effect and behavior of the bubbles inside and over the heaters. Two glass condensers are used for condensing of the vapor and they designed to be sure that all vapor become liquid and not scaping from the system.

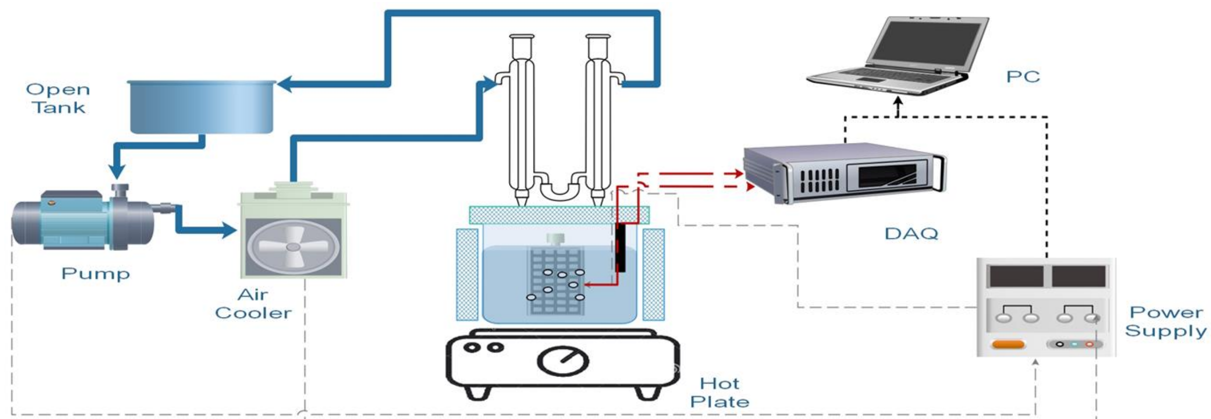

Figure 30: schematic of open bath test cell

The glass condensers are connected to the air cooler to provide enough cooling for the condensation. The air cooler can provide up to 200 Watts cooling capacities. In addition, a tank is designed in the system to remove air bubbles from the cooling system and a pump is designed in the system to circulate water inside the cooling circuit. Figure 31 shows the cooling system of the test cell.

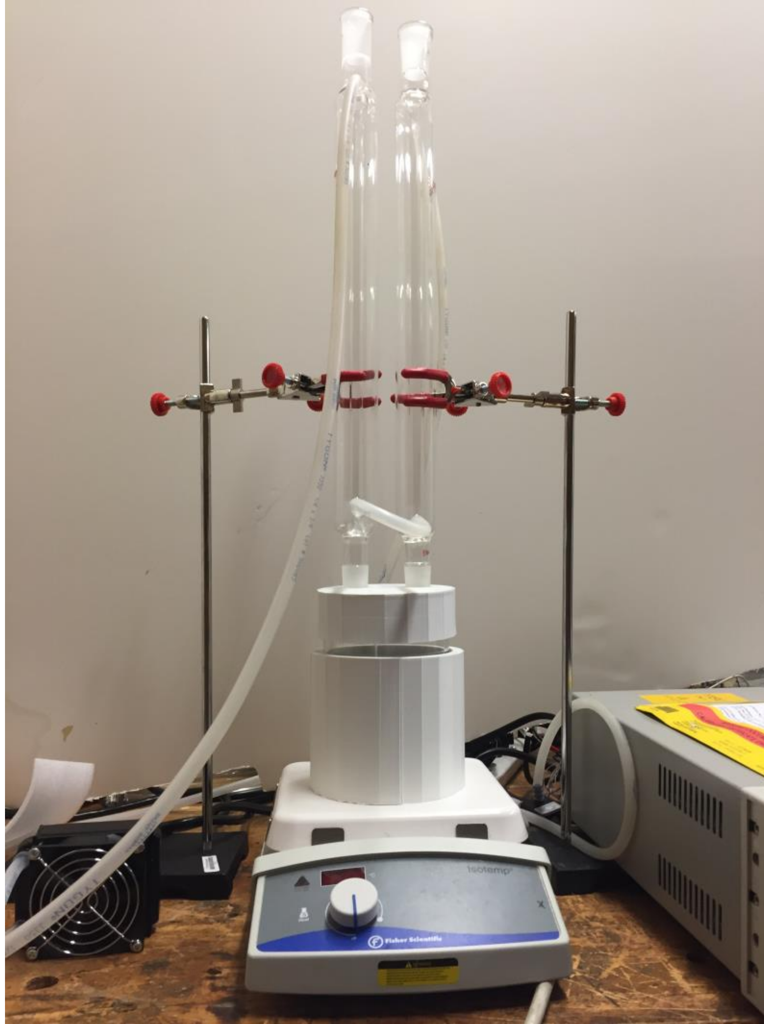

Figure 31: designed test cell for open bat immersion cooling test

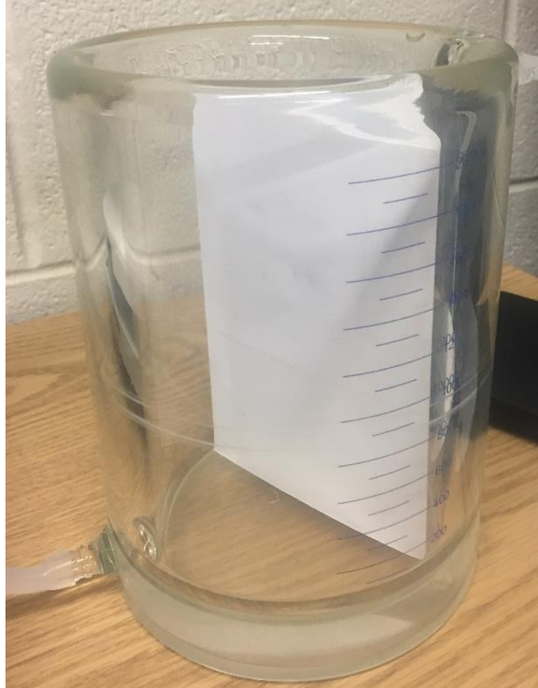

To simulate the processor and dyes of electronics systems, a heater which is simply a plate heater is used in the system. The size of this heater is 10mmx10mm and the resistance of this heater is 10 ohm and 2.5 ohm. To do test and measuring temperature and preserving heater from burning in the liquid, a copper plate is installed on the top of the heater.

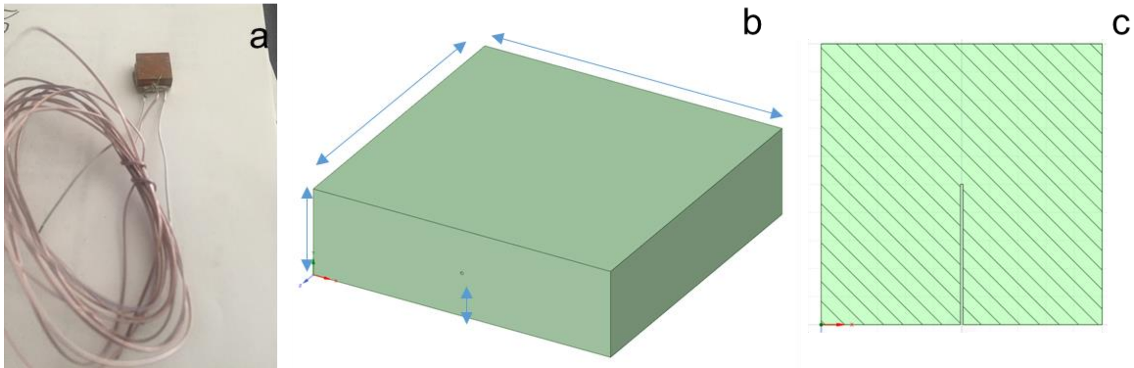

Figure 32: designed copper plate as simulated processor

Figure 32 shows the designed copper plate which is used as simulated processor. The copper plate is cube with the size of 10mmx10mmx3mm and a hole is drilled to the center of plate to place a thermocouple. This thermocouple will be used to measure the surface temperature of the plate. Then the heater and copper plate are sandwiched with silver glue. The silver glue is used due to high thermal conductivity (about 9 W/mK) which guarantees that the heat can pass from heater to copper plates. because most of the glues have low thermal conductivity (about 0.1 W/mK) and they make high thermal resistance in the system which leads to force heat flow from the other sides of the heaters. Also, the same glue is used to fix the thermocouple inside the hole. The thermocouples were calibrated by the test with ice-water mixing temperature and water boiling temperature of the water. Due to coordinate and height of the lab (Arlington, Texas[36]) where the experiment is done, the pressure is almost

atmospheric pressure and the icing and melting temperature of the water is almost the standard values.

As a simulated processor, a heater with a frame is deigned. The frame is made of the PTFE Teflon. The Teflon material has good resistivity against temperature in the experiment temperature range. In addition, the Teflon has low thermal conductivity (about 0.1) which can guarantee not to have boiling at the back of the heaters. Also, the space between heater and the frame is filled by epoxy resin. Epoxy thermal conductivity is similar to Teflon and it can secure that we will not have any boiling in any region.

Figure 33 left shows the cross section of the heater, copper block, epoxy and the Teflon frame. Table 4 presents the thermal conductivity of the material used in the frame of the heater. All material was selected to have low thermal conductivity. Figure 33 right shows the simulation done on the heater and frame. As the figure depicts, the heat mostly passes through the copper plate and less than a percent of the heat wastes through other walls. For this simulation, the heat generation boundary was considered for the heater and the rest of the walls assumed to have convection. For the convection heat coefficient, the lowest heat convection coefficient of boiling was considered.

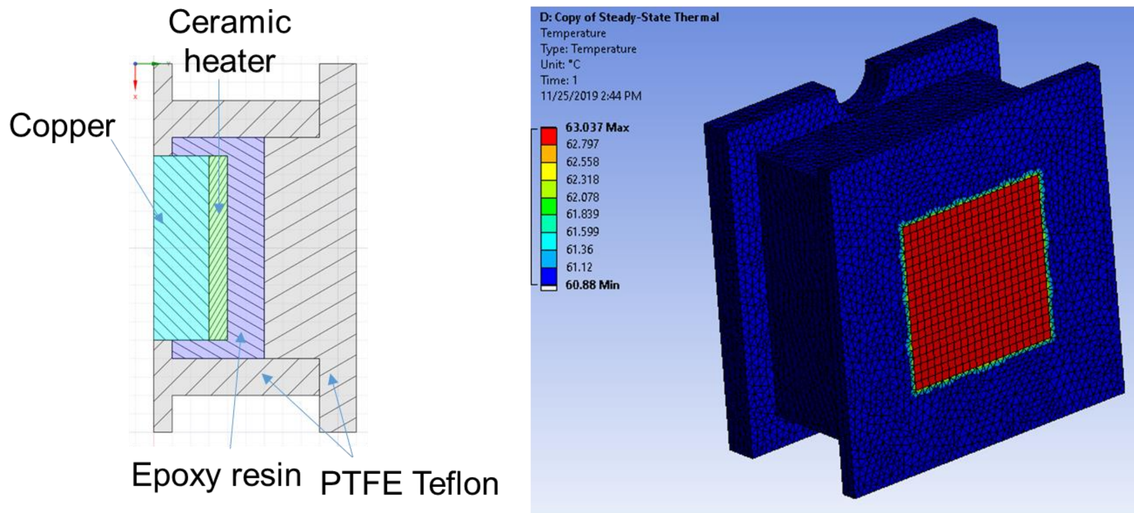

Figure 33: right, the cross section of heater and frame. Left, simulation of the design frame.

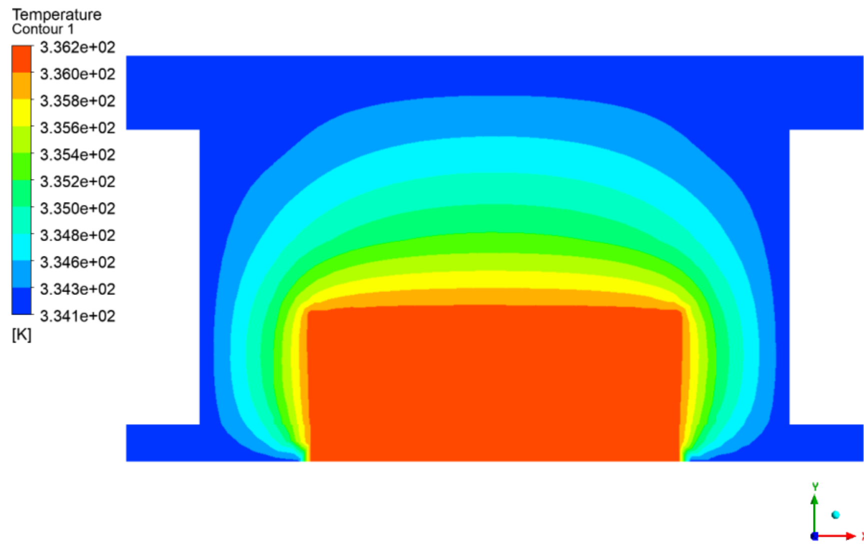

Figure 34: the isothermal lines through middle of the heater and heater frame

Table 4: thermal conductivity of material used in the heater frame

Material	Thermal conductivity (W/m-c)
Copper	380
Ceramic	180 - 200
Epoxy resin	0.15-0.25
PTEFE Teflon	0.25

One of the most important parameters in boiling is the surface roughness of the surface. The surface roughness can increase the CHF of the system. The roughness has two effects on boiling curve. First, it makes the more surface area for heat transfer and the second is that the it can keep enough liquid close to the surface for boiling.

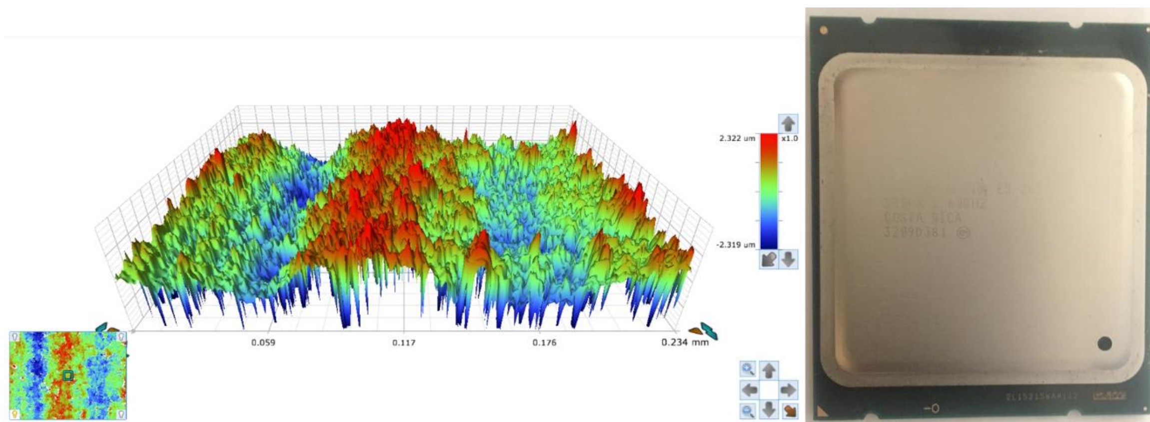

Figure 35: surface roughness of an intel Xeon CPU

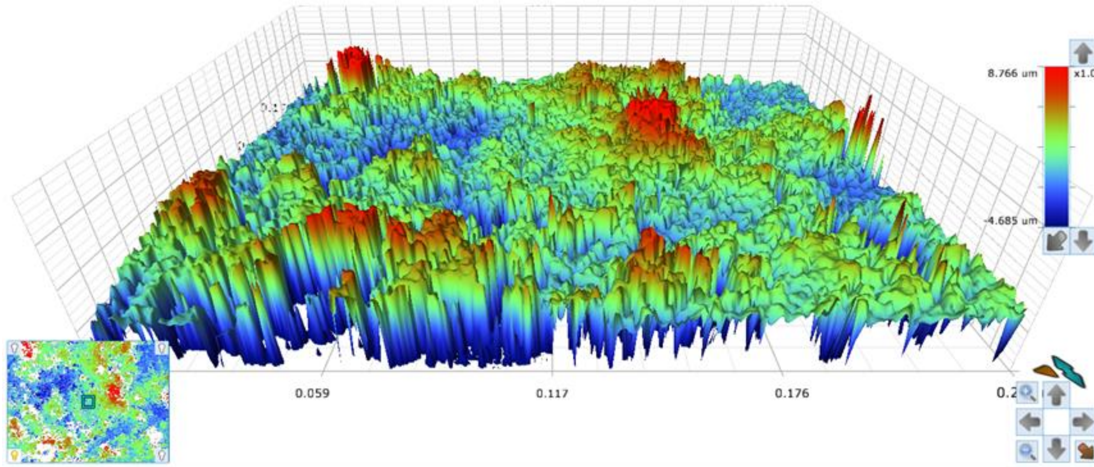

Figure 36: surface roughness of copper plate before polish

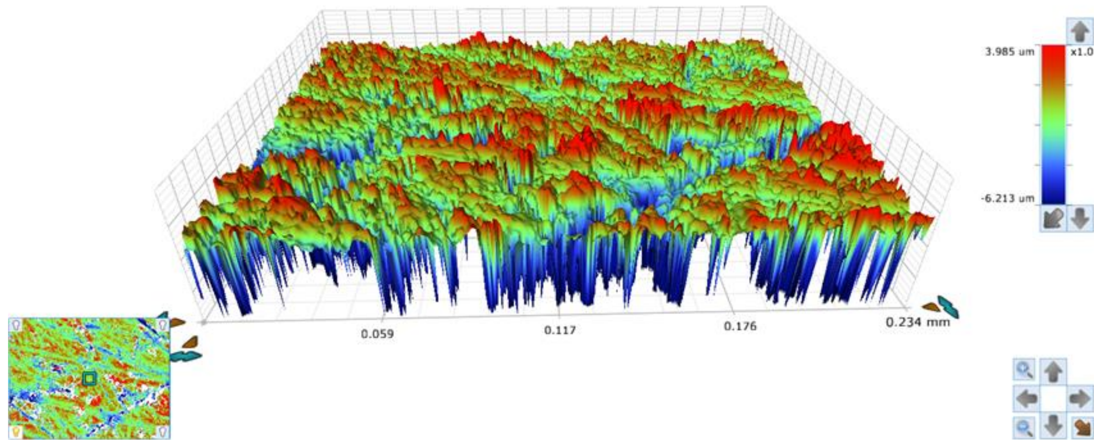

Figure 37: surface roughness of copper plate after polish

Surface roughness was measured using an optical equipment which by taking photo of the surface and image processing can specify the roughness. Figure 35 shows the roughness an Intel Xeon CPU surfaces. This surface has average

roughness close to the 400 microns. To simulate a real surface of the CPU, at first the roughness of the copper plate was measured. Figure 36, the surface roughness of the copper plate and the roughness was about the 800 microns. Therefore, the surface was polished with very fine sandpaper. After polishing, measuring was done to check the roughness of the surface and the average roughness was about 405 microns which is close to the CPU surface.

3.1. Results

In this section the results of experiments will be presented. The experiments were done for the horizontal, vertical with thermal shadowing, vertical with thermal shadowing in confined space and 3D printed surface. For all test, the target parameters are subcooled temperature and superheat temperature which are calculate by these formulas:

$$Subcooledtemp = T_{sa} - T_{sat}$$

$$Superheat\ temp = T_{wall} - T_{sat}$$

3.1.1 Horizontal uncontrolled bath

For the first case, a heater was placed horizontally in the bath and the temperature of the bat did not control to see the effect of the heater and cooling efficiency due to the heater. To run the case, the power supply was started from 0 W and increase it step by step very slowly. Because if the power increases suddenly, it can make short circuit in the heater. For each test point, we stayed 30 minutes to be sure the bath and the heater is in the steady state condition. Figure 38 shows the bubble formation due to 1 W/cm^2 of the heat generation. We have small bubble on the surface of the copper plates. Figure 39 shows the bubble on the surface of copper plate for the 4 W/cm^2 case. Compare to last case the effective area are larger and the bubble densities were increased as well. Figure 40 shows the bubble column for the case of 10 W/cm^2. For this case, the entire surface of the copper is covered by the bubbles and the bubble formation rate is very high and this case is almost close to critical heat flux of this geometry.

Figure 38: bubble generation on the plane surface for the power density (1 W/cm^2)

Figure 39: bubble generation on the plane surface for the power density (4 W/cm^2)

Figure 40: bubble generation on the plane surface for the power density (10 W/cm^2)

Table 5 shows the result for the uncontrolled bath. For this case, the boiling happens at subcooled condition. subcooled condition happens when we have boiling below boiling point. For the power density of the 0.1, the bath temperature is 39C and the superheat temperature of the surface is -36. For the high-power density which is 10, the bath subcooled temperature reaches to 12 C and the superheat temperature reaches to 9C.

Table 5: comparison of the uncontrolled bath temperature

Power density (W/cm2)	**0.1**	**1**	**2**	**3**	**4**	**5**	**6**	**10**
Superheat temp. K	-36	-22	-17	-14	-6	0	3	9
Subcooled temp. K	39	38	37	34	30	28	24	12

3.2. Thermal Shadow experiment

In cooling with air, the effect of the thermal shadowing is large. Thermal shadowing happens when the second equipment is in the way of thermal boundary layer of the first equipment. If the design does not consider this, the temperature of the second equipment can reach the limitations and it can be burn. To test this, two heaters were placed vertically in the frame therefore the bubble of bottom heater will cover the top heater. For this test, the temperature of the bath was controlled and kept as boiling temperature.

Figure 41: bubble generation on the vertical configuration of the plane surface for the power density 4 W/cm^2

Figure 41 shows the bubble formation and boundary layer over the two heaters. As the figure shows, the generated bubble covers the top heaters. These bubbles have higher velocity compare to the bottom heater. Figure 42 shows the boiling characteristic curve for the top and bottom heaters. As it shows the top heater is colder due to high speed of the bubbles. Therefore, the top surface has higher convection coefficient.

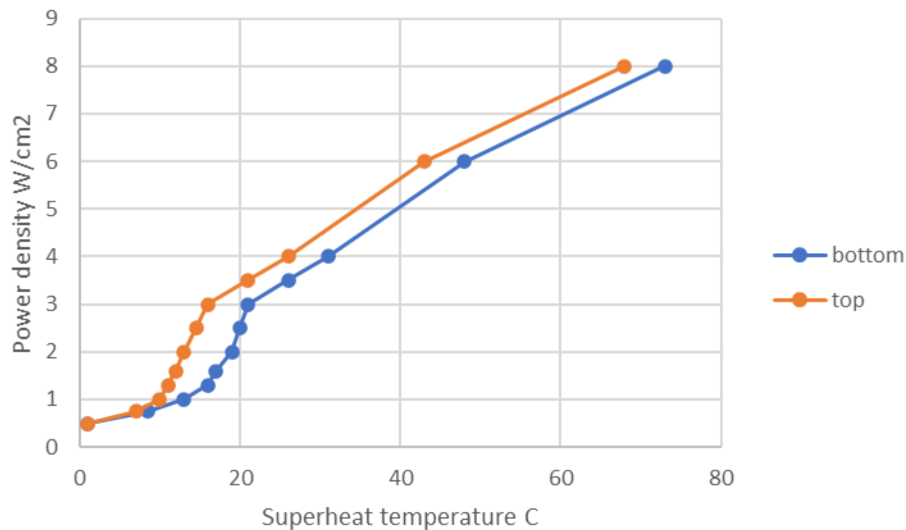

Figure 42: boiling characteristic curve for vertical configuration

3.3. Confined space

One of the important questions is how close we can place two servers. This way we can increase the rack densities and this way we can decrease the investment on the cooling because the liquid is quite expensive and this way, we can reduce the amount of cooling that we need.

Figure 43: vertical configuration with confined space made with glasses

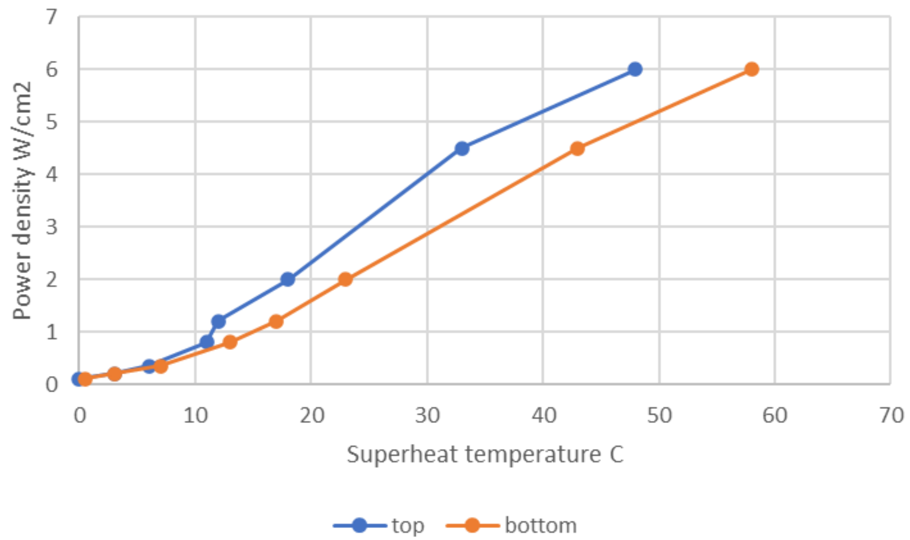

Figure 44: boiling characteristic curve for vertical configuration with confined space

Figure 43 shows the configuration and set-up of the heaters in confined space. The space was made with a glass covers the face of heaters and the space was kept by wooden sticks. For this test, the temperature of the bath was controlled and kept as boiling temperature. Figure 44 shows the results of the test. As the curve shows, in the beginning, we have the same temperature because the bubble generation is not high and after that the temperature of the top heater is colder than the bottom heater.

3.4. 3D printed surface

To increase the boiling efficiency enhancing a surface roughness or adding a porosity is one of the popular ways. But making a uniform and stable surface is not easy on the boiler surface. With the help of 3D printing, we can make engineer surfaces and every time we can have homogenous surface. For this purpose, the power and the speed of printing were changed to reach the best surface. Figure 45 shows the sample of 3D printed surface, we tried to print a net on the surface of the boiler to make high roughness surface. Figure 46 shows the boiling characteristic curve of the test. As the curve shows the 3D printer heater has higher efficiency compare to the plane surface but it needs more enhancement.

Figure 45: 3D printed surface with high roughness to increase the efficiency

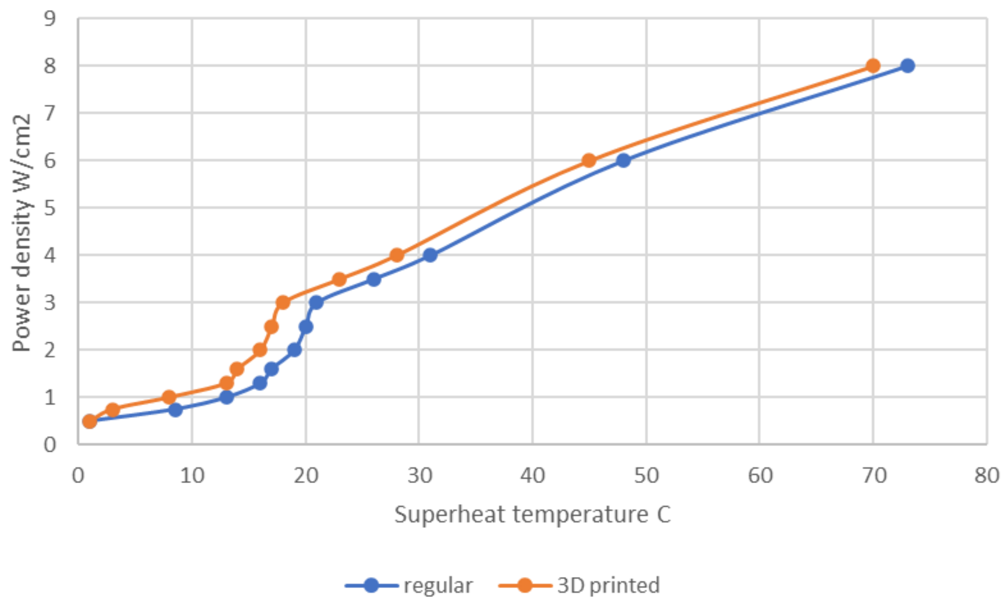

Figure 46: comparison of the 3D printed enhanced surface with plane surface

3.5. Conclusion

The immersion cooling of the equipment was tested using heaters in open bath and it was found that thermal shadowing does not happen in two phase cooling and also, it helps to have higher cooling efficiency. Also, the confined space can decrease cooling efficiency but the optimum space should be found. Finally, the 3D printed part was tested and it was found that it can enhance the efficiency but further research and testing needed to find the optimum surface.

References

[1] “Immersion Cooling for Green Computing,” presented at the OCW.

[2] D. Cheney, “High Performance Go Workshop,” Apr. 26, 2019. https://dave.cheney.net/high-performance-go-workshop/gopherchina-2019.html.

[3] D. Sartor, “Partnering with DOE to Improve Data Center Efficiency,” presented at the FEDERAL UTILITY PARTNERSHIP WORKING GROUP SEMINAR, Savannah, Georgia, Apr. 12, 2017, [Online]. Available: https://www.energy.gov/sites/prod/files/2017/04/f34/fupwg_spring17_sartor.pdf.

[4] S. V Patankar, “Airflow and Cooling in a Data Center,” *J. Heat Transf.*, vol. 132, no. 7, pp. 73001–73017, Apr. 2010.

[5] R. Miller, “Facebook Unveils Custom Servers, Facility Design,” *datacenter knowledge*. https://www.datacenterknowledge.com/archives/2011/04/07/facebook-unveils-custom-servers-facility-design.

[6] grccoling, “Liquid Immersion Cooling for Data Centers,” Jul. 03, 2019. https://www.grcooling.com/ 0.

[7] “PASSIVE COLDPLATE LOOP.” https://www.coolitsystems.com/passive-coldplate-loop/.

[8] “Advanced Cooling - A Large Scale Deployment Experience Using Immersion Cooling,” presented at the OCP summit 2019, 2019.

[9] J. Fathi Sola, F. Alinejad, F. Rahimidehgolan, and A. Niazmand, “Fatigue life assessment of crankshaft with increased horsepower,” *Int. J. Struct. Integr.*, vol. 10, no. 1, pp. 13–24, Jan. 2019, doi: 10.1108/IJSI-04-2018-0020.

[10] Submer, “What is Immersion Cooling?,” Jul. 03, 2019. https://submer.com/blog/what-is-immersion-cooling 0.

[11] A. Jaikumar and S. Kandlikar, “Enhanced Pool Boiling For Electronics Cooling Using Porous Fin Tops on Open Microchannels With FC-87,” *Appl. Therm. Eng.*, vol. 91, Aug. 2015, doi: 10.1016/j.applthermaleng.2015.08.043.

[12] S. J. Thiagarajan, R. Yang, C. King, and S. Narumanchi, “Bubble dynamics and nucleate pool boiling heat transfer on microporous copper surfaces,” *Int. J. Heat Mass Transf.*, vol. 89, pp. 1297–1315, Oct. 2015, doi: 10.1016/j.ijheatmasstransfer.2015.06.013.

[13] M. S. El-Genk and J. L. Parker, “Nucleate boiling of FC-72 and HFE-7100 on porous graphite at different orientations and liquid subcooling,” *Energy Convers. Manag.*, vol. 49, no. 4, pp. 733–750, 2008, doi: https://doi.org/10.1016/j.enconman.2007.07.028.

[14] J. Y. Chang and S. M. You, “Enhanced boiling heat transfer from microporous surfaces: effects of a coating composition and method,” *Int. J. Heat Mass Transf.*, vol. 40, no. 18, pp. 4449–4460, Nov. 1997, doi: 10.1016/S0017-9310(97)00057-4.

[15] S. B. White, A. J. Shih, and K. P. Pipe, “Boiling surface enhancement by electrophoretic deposition of particles from a nanofluid,” *Int. J. Heat Mass Transf.*, vol. 54, no. 19, pp. 4370–4375, Sep. 2011, doi: 10.1016/j.ijheatmasstransfer.2011.05.008.

[16] K. N. Rainey and S. M. You, “Pool Boiling Heat Transfer From Plain and Microporous, Square Pin-Finned Surfaces in Saturated FC-72,” *J. Heat Transf.*, vol. 122, no. 3, pp. 509–516, Aug. 2000, doi: 10.1115/1.1288708.

[17] D. E. Kim, D. I. Yu, D. W. Jerng, M. H. Kim, and H. S. Ahn, "Review of boiling heat transfer enhancement on micro/nanostructured surfaces," *Exp. Therm. Fluid Sci.*, vol. 66, pp. 173–196, Sep. 2015, doi: 10.1016/j.expthermflusci.2015.03.023.

[18] A. Kraus and A. Bar-Cohen, "hermal analysis and control of electronic equipment,"," *Hemisphere Publ. Corp*, vol. 1, p. 633, 1983.

[19] "Two-Phase Liquid Immersion Cooling." https://www.gigabyte.com/Solutions/Cooling/immersion-cooling.

[20] "About 3M™ Novec™." https://www.3m.com/3M/en_US/novec-us/.

[21] N. Shiro, "The maximum and minimum values of the heat q transmitted from metal to boiling water under atmospheric pressure," *Int. J. Heat Mass Transf.*, vol. 27, no. 7, pp. 959–970, Jul. 1984, doi: 10.1016/0017-9310(84)90112-1.

[22] J. Gess, "Experimental Investigation of a Liquid Immersion Cooled Electronics Module using Two-Phase Heat Transfer for Thermal Management," Auburn university, Alabama, 2015.

[23] B. Ramakrishnan, "Viability of Server Module Thermal Management Using Enhanced Heat Sinks and Low Global Warming Potential Dielectric Fluids," MS Thesis, Auburn university, Alabama, 2014.

[24] M. S. El-Genk, “Nucleate Boiling Enhancements on Porous Graphite and Microporous and Macro–Finned Copper Surfaces,” *Heat Transf. Eng.*, vol. 33, no. 3, pp. 175–204, Feb. 2012, doi: 10.1080/01457632.2011.589305.

[25] A. Sridhar, “Experimental Evaluation of Immersion-Cooled Strategies for High-Power Server Modules,” MS Thesis, Auburn university, Alabama, 2012.

[26] T. Ren, C. Yan, M. Yan, and S. Yu, “CFD Analysis on Wall Boiling Model During Subcooled Boiling in Vertical Narrow Rectangular Channel,” Volume 8: Computational Fluid Dynamics (CFD); Nuclear Education and Public Acceptance, Jul. 2018, doi: 10.1115/ICONE26-81554.

[27] B. G. Dehkordi, S. Fallah, and A. Niazmand, “Investigation of harmonic instability of laminar fluid flow past 2D rectangular cross sections with 0.5–4 aspect ratios,” *Proc. Inst. Mech. Eng. Part C J. Mech. Eng. Sci.*, vol. 228, no. 5, pp. 828–839, Jun. 2013, doi: 10.1177/0954406213491906.

[28] B Ghadiri Dehkordi, A Niazmand, and S Soheili, “Study the Consistency of k-ε and Smagorinsky Models in Simulation of Circular Cylinder,” presented at the The 10th Iranian Aerospace Society Conference, 2011.

[29] Amirreza Niazmand, “Large eddy simulation of internal incompressible turbulent flow using structure sub-grid eddy viscosity model in a lid driven cavity,” 2011.

[30] V. H. Del Valle and D. B. R. Kenning, “Subcooled flow boiling at high heat flux,” *Int. J. Heat Mass Transf.*, vol. 28, no. 10, pp. 1907–1920, 1985, doi: https://doi.org/10.1016/0017-9310(85)90213-3.

[31] G. Kocamustafaogullari and M. Ishii, “Foundation of the interfacial area transport equation and its closure relations,” *Int. J. Heat Mass Transf.*, vol. 38, no. 3, pp. 481–493, 1995, doi: https://doi.org/10.1016/0017-9310(94)00183-V.

[32] G. Kocamustafaogullari and M. Ishii, “Interfacial area and nucleation site density in boiling systems,” *Int. J. Heat Mass Transf.*, vol. 26, no. 9, pp. 1377–1387, 1983, doi: https://doi.org/10.1016/S0017-9310(83)80069-6.

[33] H. C. Unal, “Maximum bubble diameter, maximum bubble-growth time and bubble-growth rate during the subcooled nucleate flow boiling of water up to 177 MN/m2,” *Int. J. Heat Mass Transf.*, vol. 19, no. 6, pp. 643–649, 1976.

[34] B. B. Mikic and W. M. Rohsenow, “A New Correlation of Pool-Boiling Data Including the Effect of Heating Surface Characteristics,” *J. Heat Transf.*, vol. 91, no. 2, pp. 245–250, May 1969.

[35] R.-H. C. Daniel P. Rini Louis C. Chow, “BUBBLE BEHAVIOR AND HEAT TRANSFER MECHANISM IN FC-72 POOL BOILING,” *Exp. Heat*

Transf., vol. 14, no. 1, pp. 27–44, Jan. 2001, doi: 10.1080/089161501461620.

[36] "Arlington, Texas," *Wikipedia, the free encyclopedia*. https://en.wikipedia.org/wiki/Arlington,_Texas.

Biography

Amir is a research assistant at EMNSPC Lab at UTA. He is pursuing a Doctoral Degree in Mechanical engineering; his research focuses on two phase immersion cooling for high power density electronics. He has substantial experience in simulation of thermo-fluidic systems using CFD methods. Previously, Amir worked as a designer of Auxiliary and Accessories system of a power generation company, and he has 2 years of teaching engineering level courses at Azad university (IAU).